

# Integration of digital filters and measurements

Jan Peter Hessling

*Measurement Technology, SP Technical Research Institute of Sweden*

## 1. Introduction

Digital filters (Hamming, 1998; Chen, 2001) are versatile, practical and effective. They can be used in most computerized applications of modern technology and science. Nearly every person in technologically developed regions daily encounter digital filters in cars, dvd-recorders, computers, telecommunication systems etc. Usually, digital filters are designed and optimized by signal processing experts for standardized tasks in specific systems. Extensive work may result in advanced and complex filters. This is motivated by massive duplication. The marginal production cost for a filter is practically zero and the development cost per unit is negligible. The advantages of using digital instead of analogue filters are often profound. Not only are the costs negligible, their flexibility makes it possible to achieve superior results. Even unstable operations can be realized by means of reversed filtering. The limitations of digital filters are mainly mathematical, rather than physical as for analogue filters.

Dynamic measurements condense observations into quantitative representations (Hessling, 2010a). Dynamic methods for improving, interpreting and assessing the quality of measurements are relatively scarce. These methods can be formulated in terms of ideal prototype systems acting on physical signals to produce the desired information. A dynamic calibration procedure is usually required to find the model from which such prototypes are determined. Ideal prototypes are approximated and optimized into realizable prototypes which can be cast into digital filters by means of sampling. These filters differ from most common filters of today. They are dedicated filters with a high level of adaptation and flexibility, designed to improve or simplify the evaluation of a wide range of measurements for many different purposes. The common denominator of all filters is that they are intended to provide a supporting link of standardized dynamic analysis between the 'raw' measurements and an inexperienced destined user. The digital filters and the measurement devices are preferably seamlessly integrated in the final application, which most often already has a computer program for administrating the measurement.

The motivation for making any measurement is to extract information. The desired information is rarely identical to measured signals. Measured signals need to be processed or analyzed. Signals may be corrected. To determine how wrong the result might be, the uncertainty needs to be estimated. The measurement system may be one part of a complex dynamic system, for instance, an accelerometer attached to a vibrating vehicle. Sometimes transformations between various points in space, or electrical quantities etc. are required. We might be interested in the consequences of measured signals. The impact of interest is

often quantified in scalar measures or *features* like peak loads in crash testing, average power in electrical systems, or accumulated risk of injury.

The analysis is based on how dynamic systems are modeled with differential equations, rather than any specific system which can be electrical, mechanical, etc. To illustrate the design, or *synthesis* and application of digital filters, mechanical systems will be used. There are two reasons for this choice: Mechanical systems are widely understood and digital filters have not yet been utilized in this field to any significant extent. The applications will be split into two categories, analysis of measured signals (section 3) and feature extraction (section 4). For analyzing measured signals the same mechanical transducer system as well as triangular input signal will be used. This example represents the simplest possible non-trivial dynamic measurement system, which is good for illustration of principles rather than details. Two examples of feature extraction are given, the analysis of road humps (section 4.1) and the determination of road surface roughness, or texture (section 4.2). Both examples relate to traffic and the structure of road surface, and both address potential health risks. The geometric scales differ: A speed limiting road hump is a 3-20 m long intentionally modified part of the road. The texture relates to unevenness of 5-50 mm wavelength. The road hump profile is translated to a time-dependent excitation signal of a bandwidth varying with the speed of passage. The surface texture example illustrates that digital filters are not limited to the time domain but work perfectly well also for space domain analysis.

The digital filters will be expressed on a standard linear-in-response finite/infinite impulse response (FIR/IIR) form for direct implementation. It will be indicated how any filter may be transferred to a state-space form for generalization into a Kalman filter (Simon, 2006).

## 2. Synthesis of digital filters from prototypes

### 2.1 General framework

The real world of observable physical quantities are almost exclusively continuous in time as well as amplitude. The world of information we are interested in may contain anything we can imagine. The link between the two is the world of computers which is discrete in time as well as amplitude. Our interest may be expressed in *prototype systems*. These hybrid systems are not generally physical, but are formulated as if they would. The prototypes for dynamic correction in section 3.2 and the sensitivity systems in section 3.3.1 are two examples. The prototypes will specify the desired filter operation completely. No conventional filter specification in terms of pass-band, stop-band and allowed ripple etc. will be used. Prototypes are widely used in filter synthesis. The concept is here further generalized to describe virtually anything we might be interested in.

The major part of this chapter will be devoted to derivation of *realizable* dynamic prototype systems *continuous in time* (CT). These prototypes are sampled to convert them into systems *discrete in time* (DT), for direct interpretation as digital filters. The translation of *any* continuous formulation to a discrete formulation will be denoted *sampling*. The terminology is here generalized to reflect symmetries: Signals, systems as well as statistical information may be sampled. The methods of sampling are rather different though. Sampling of signals is unique. Sampling of systems necessarily adds distortion and there is a multitude of different well-known methods. *Random sampling* of statistical information is practiced in Monte Carlo simulations (Metropolis, 1949; Rubenstein & Kroese, 2007) but there are other recent and more effective methods of *deterministic sampling* (Julier & Uhlmann, 2004).

Sampling is here lifted to a more abstract level since statistical information is neither physical, nor directly observable. Statistical dynamic models may be sampled twice: The statistical information is first sampled to obtain a finite set of CT prototype systems. Each prototype system is then sampled to find a corresponding digital filter. Sampling of CT systems will always render systematic model errors. These will be called *discretization time errors* (DTE) (Hessling, 2008a). The DTE is different for different input signals and may thus be visualized in various ways, depending on the chosen measure of signal error. If the DTE is given as a function of system bandwidth, the *utilization* of a mapping expresses how much of the maximum (DTE=0) bandwidth that may be used for acceptable DTE. The theoretical limit is set by the sampling rate  $f_s = T_s^{-1}$  which results in a maximum bandwidth given by the Nyquist frequency  $f_N = f_s/2$ . For many prototypes though there may be other lower bandwidth limits, for instance the limit of unacceptable noise amplification. *Reversed* or backward digital filtering is an allowed luxury for analyzing measurements. It simplifies many tasks like stabilization and elimination of phase distortion tremendously and will be used extensively. Reversed filtering is implemented in three steps: 1. The beginning and the end of the signal are exchanged to 'reverse direction'. 2. Forward filtering 3. Repetition of step 1. *Symmetric* forward and reverse filtering (Gustafsson, 1996) is in its simplest form (Hamming, 1998) implemented as repeated filtering in both directions. The fall-off rate as well as the attenuation at the nominal cross-over frequency is doubled compared to forward filtering. The total phase response vanishes identically (at all frequencies).

The methods for sampling of prototype systems fall into two categories, numerical sampling and *mapping* techniques. Numerical sampling minimizes the discrepancy between characterizations of the CT prototype and the sampled DT model (Elster et al., 2007). The characterizations may be given in any representation, for instance in the time or frequency domain. The deviation is often quantified with a weighted least square error (Bjork, 1996). Splitting system identification of CT models (Pintelon & Schoukens, 2001) and numeral sampling into successive steps of analysis is strongly discouraged: The two operations are comparable and better optimized jointly, as is conventional (Ljung, 1999). Mapping techniques are based on universal relations between CT and DT models and it is simple to switch sampling rate. Robustness and simplicity are paid with a minor reduction of accuracy due to lack of optimality of the mapping rule. The accuracy is determined by the calculated DTE, and controlled by the selection of mapping. A brief recapitulation of some mappings and their properties are given in the next section.

## 2.2 Mappings for sampling of prototypes

A common class of mappings samples the response of the CT prototype system to an input signal of particular interest. The calculated CT response is sampled like any signal to yield a DT system which does not distort, or is *invariant* with respect to the selected input signal. The *impulse invariance* method (IMP) (Chen, 2001) samples the impulse response  $h(t)$ . The calculation is facilitated by expansion in residues  $r_k$  and poles  $p_k$ ,

$$H(s) = \frac{\prod_k (s - z_k)}{\prod_k (s - p_k)} = \sum_k \frac{r_k}{s - p_k} \Rightarrow h(t) = \sum_k r_k \exp(p_k t). \quad (1)$$

Sampling with sampling time interval  $T_S = f_S^{-1}$  results in the DT impulse response  $g_n$  and transfer function  $G(z)$ ,

$$g_n = h(nT_S) = \sum_k r_k \exp(np_k T_S) \Rightarrow G(z) = T_S \sum_n g_n z^{-n} = \sum_k \frac{r_k T_S z}{z - \exp(p_k T_S)}. \quad (2)$$

The IMP method requires a decaying frequency response  $H(i\omega) \approx 0, \omega > \pi f_S$  to avoid aliasing. Thus it can only be used if the number of poles of the CT prototype exceeds its number of zeros. The static amplification is *not* preserved, see Fig. 1 (left). Poles of the CT system are mapped to poles of the sampled DT system with an exponential mapping  $p_k \rightarrow \exp(p_k T_S)$ . The zeros of the two systems have no simple relation, not even their number is preserved. If instead also zeros are mapped like the poles of the IMP method, the exponential pole-zero mapping (EXP) results (Chen, 2001; Hessling, 2008a),

$$q_k \rightarrow \exp(q_k T_S), \quad q_k = z_k \cdot p_k. \quad (3)$$

This simple mapping preserves the static amplification, the numbers of poles and zeros as well as the stability properties. The high frequency amplification is bounded. Its major drawback is a fairly low utilization. The mapping is transparent as the underlying CT model in the s-plane can be discerned in the z-plane. This will be the default mapping.

'Functional' mappings are described by substitution rules  $s = M(z)$ . The DT transfer function  $G(z)$  is found from the CT transfer function  $H(s)$  as  $G(z) = H(M(z))$ . It is important to compensate for the time delays  $\tau_G, \tau_H$  of the DT and CT systems, respectively. The delays should conform to the measure of the DTE. If the DTE  $\Delta H$  is expressed in the frequency domain,  $\Delta H = \exp(i\omega\tau_G)G(\exp(i\omega T_S)) - \exp(i\omega\tau_H)H(i\omega)$ . The standard bi-linear mapping (BIL) (Chen, 2001) is a functional mapping,

$$s = \frac{2(z-1)}{T_S(z+1)}. \quad (4)$$

The BIL mapping unfortunately introduces singularities at the Nyquist frequency ( $z = -1$ ). It also results in a non-linear mapping of the frequency axis called *frequency warping* (Chen, 2001).

Since  $s = M(z)$  is the differential operator and  $z$  the translation operator, the mapping function is nothing else than a discrete time approximation of a simple derivative expressed in translations. The symmetric difference quotient approximation  $\partial_t f(t) \approx [f(t+T_S) - f(t-T_S)]/2T_S$  directly renders the mapping  $s = (z - z^{-1})/2T_S$ . A novel  $n$ -th order symmetric approximation is obtained by expanding in symmetric difference quotients of various integer steps  $k$ ,

$$M^{(n)}(z) = \sum_{k=1}^n c_k^{(n)} \frac{z^k - z^{-k}}{2kT_S}. \quad (5)$$

The coefficients  $c_k^{(n)}$  may be found by minimizing the DTE over the whole frequency axis up to the Nyquist frequency using linear regression for the approximation,

$$1 \approx \sum_{k=1}^n c_k^{(n)} \frac{\sin(kx)}{kx}, \quad x \in [0, \pi]. \tag{6}$$

A low-frequency approximation is found by expanding the sine-function and matching as many powers as allowed by the order  $n$ . This yields a whole sequence of difference quotient mappings  $DQ(n)$ . The DTE decreases rapidly with  $n$ , but the number of poles and zeros increases with a factor of  $2n$ .

The choice of method for sampling prototypes is in practice influenced by many aspects. It should be stressed that the DTE seldom is the only relevant issue. The discussion of various mappings for sampling of prototype systems is concluded with an illustration of the DTE (Fig. 1), for the example model described in section 3.1.1.

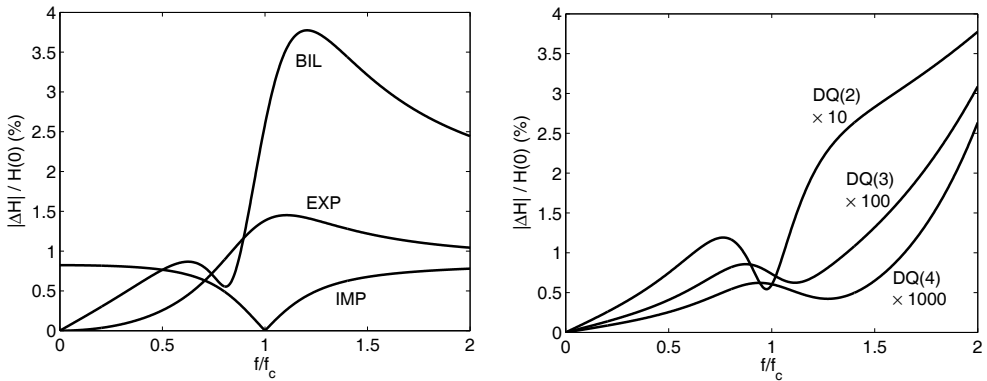


Fig. 1. The normalized DTE for the transducer model (Eq. 11) and various mappings (notation is given in the text). The mappings  $DQ(n)$  are rescaled for comparison (right).

**2.3 State space formulation for Kalman filter**

Kalman filters are popular tools for optimal estimation of signals in noisy measurements (Simon, 2006). Conventional digital filters are closely related to Kalman filtering. In this section it will be briefly indicated how any digital filter can be converted into the formulation used for Kalman filters.

Kalman filters utilize DT state-space equations, which are equivalent to transfer functions. State-space equations exist for both CT and DT and are not uniquely specified by the system. Their main feature is linearity in the differential  $\partial_t$  (CT) or displacement operator  $\Delta$  (DT). State-space equations are convenient for analyzing large and complex multiple-input multiple-output systems, like finding the response of vehicles (section 4.1.2), using linear algebra. Sampling of CT state-space equations can be made by transformation to transfer functions, sample (section 2.2) and transform to DT state-space equations.

A state-space formulation contains two equations, a dynamic state-space equation and a static measurement equation. The state-space equation is the 'engine' that drives the system in response to its input. The measurement equation describes how our quantity of interest is related to the state-space variables and the input. This separation makes it possible to use virtually any set of [state-space] variables. They may be physical quantities but often are not. The key aspect of all sets of variables is that they split the model into several equations linear in the differential  $\partial_t$  (CT) or displacement  $\Delta$  (DT) operator. In CT,

$$\begin{aligned} \partial_t u &= Au + Bx \\ y &= Cu + Dx \end{aligned} \quad (7)$$

The input  $x$ , the output  $y$  and the state-space variables  $u$  are all column vectors. Applying the La-place transform, the transfer function is obtained by matrix inversion,

$$H(s) = \frac{Y(s)}{X(s)} = [C(s - A)^{-1}B + D] = \sum_{k=0}^m b_k s^k \bigg/ \sum_{k=0}^n a_k s^k. \quad (8)$$

This transformation from any linear state-space formulation to the corresponding transfer function non-linear in  $s$  is unique. The set of canonical state-space variables is one of many choices of transformation in the opposite direction. This choice must however be extended to allow for prototypes with  $m > n - 1$  (subscripts indicate sizes of sub-matrices),

$$\begin{aligned} U_1(s) &= s^m X(s) \bigg/ \sum_{k=0}^n a_k s^k & A &= \begin{pmatrix} 0_{(1 \times (m-n+1))} & -a_{n-1}/a_n & -a_{n-2}/a_n & \cdots & -a_0/a_n \\ & \text{diag}(1)_{(m \times m)} & & & 0_{(m \times 1)} \end{pmatrix} \\ U_k(s) &= \begin{cases} \frac{1}{s} U_{k-1}(s), \\ k = 2, 3, \dots, m+1 \end{cases} & \Rightarrow B &= (1 \ 0 \ \cdots \ 0)^T \\ & & C &= (b_m \ b_{m-1} \ \cdots \ b_0) \\ & & D &= 0 \end{aligned} \quad (9)$$

The transformations are similar for DT, essentially let  $\partial_t \rightarrow \Delta$  and  $s \rightarrow z$ . The noise enters as process noise ( $w$ ) in state variables as well as measurement noise ( $v$ ) in the measured quantity. The process noise effectively corresponds to the uncertainty of our model (section 3.3), but is expressed differently. Depending on the state variables it may be difficult to assign a reasonable model of process noise in any other way than studying the result. The measurement noise is physical and observable and therefore much easier to estimate. Adding noise in the DT state-space model we finally arrive at the Kalman filter equations,

$$\begin{aligned} \Delta u &= Au + Bx + w \\ y &= Cu + Dx + v, \quad \Delta u_k = u_{k+1}. \end{aligned} \quad (10)$$

### 3. Applications related to calibration

The result of a dynamic calibration of a measurement system is difficult to use directly (Hessling, 2010a). The performance of the system depends strongly on the variation of the signal and has to be calculated for *every* measured signal. Parts of this calculation can be formulated as digital filtering of measured signals. The time-invariant unique filters are then synthesized from the calibration result. The filter coefficients *represent* the calibration result. Digital filters are already used in some measurement systems. The novel aspect here is to use digital filtering as a method to formulate the calibration result for every measured signal. Digital filters will here be used for dynamic correction (section 3.2) and for estimating the model uncertainty of this correction (section 3.3).

The measured signal results from the specific combination of input signal and measurement system. The statistical dynamic model of the measurement system will be assumed time-invariant and linear-in-response, but non-linear-in-parameters. The variable performance is due to the time-dependence of the signal and not the system. Of primary interest is to correct the measured signal to resemble the physical input of the measurement system as much as possible. That is an inverse problem, as it requires the construction of a prototype for the inverse system. The uncertainty of the model is transferred to uncertainty of this prototype of correction. When applying the correction filter, the uncertainty of the corrected signal increases further due to measurement noise. Thus there are two principal sources of uncertainty for corrected signals, model uncertainty and noise. For the addressed linear-in-response systems the measurement noise and the measured signal propagate identically through the correction filter. Propagation of measurement noise will not be addressed here as it only relates to the correction filter and is elementary (Hessling, 2009). The model uncertainty propagates very differently – a perturbation of a dynamic model leads to a non-trivial perturbation of the corrected signal.

#### 3.1 Example of measurement

##### 3.1.1 Measurement system

The model of a measurement may be determined from calibration and/or from first principles. First principles often suggest structures of the model while the values of the parameters are deduced from experimental calibration data by means of system identification (Ljung, 1999; Pintelon & Schoukens, 2001). To focus on synthesis of digital filters rather than modeling, a strongly simplified model will be used. Mechanical sensors for measuring acceleration, pressure, force and torque are often made of a strain-gauge element attached to a flexible sensor material. The mechanical construction is well described by two masses separated by a damped spring (Crosswy & Kalb, 1970). This results in a simple resonance at frequency  $f_c$  with relative damping  $\zeta$ . Usually the damping is moderate ( $\zeta < 1$ ) (Moghisi & Squire, 1980) giving a complex-conjugated pole pair  $(p, p^*)$  in the s-plane,

$$H(s) = \frac{K|p|^2}{(s-p)(s-p^*)} = \frac{r_1}{s-p} + \frac{r_2}{s-p^*}, \quad \begin{aligned} p &= 2\pi f_c \left( -\zeta \pm i\sqrt{1-\zeta^2} \right) = p_R + ip_I \\ r_k &= i(-1)^k K|p|^2 / 2\text{Im}(p) \end{aligned} \quad (11)$$

The mean  $\langle \cdot \rangle$  and the covariance matrix for the parameters are given in Table 1. The complex-valued frequency response is given by  $H(i\omega)$ . The first parameterization is made in  $K$  and the roots, or poles ( $p$ ) of the denominator polynomial, rather than its coefficients. This factorization makes the models less non-linear-in-parameters. The high sensitivity to variations in coefficients would make the estimation of measurement uncertainty (section 3.3) more difficult. These problems increase rapidly with the order of the model. The second parameterization is made in residues ( $r$ ) and poles. All models are linear in residues. Exploring different parameterizations is strongly encouraged as that may improve and simplify the analysis significantly. Since the input as well as output signal of the measurement system is real-valued, poles and zeros are either real, or complex-conjugated in pairs. This physical constraint must be fully respected in all steps of the analysis. The simple transducer model has only one complex-conjugated pole pair but that is sufficient for illustrating the various methods. The general case with an arbitrary number of poles and zeros is discussed in recent publications (Hessling, 2008a; 2009).

$$\left( \begin{matrix} \langle K \rangle \\ \langle f_C \rangle \\ \langle \zeta \rangle \end{matrix} \right) = \left( \begin{matrix} 1.00 \\ 50.0 \text{ kHz} \\ 0.300 \end{matrix} \right), \quad \text{cov}(K, p_R, p_I) = 10^{-4} \begin{pmatrix} 0.50^2 & 0 & 0 \\ 0 & 1.00^2 & 1.20^2 \\ 0 & 1.20^2 & 2.00^2 \end{pmatrix}, \quad \begin{matrix} S/N = 50\text{dB} \\ f_s = 20f_C \end{matrix}$$

Table 1. Mean values and covariance matrix of the parameters of the dynamic model (Eq. 11), signal-to-noise ratio  $S/N$  at zero frequency, and chosen sampling rate  $f_s$ .

### 3.1.2 Input and output signal

The performance of the measurement system is different for different physical input signals. For illustration it is sufficient to study only one input signal. In order to obtain visible effects, its bandwidth is chosen high. Its regularity or differentiability should also be low as that implies a high sensitivity to the proposed filtering. The triangular pulse in Fig. 2 fulfills these requirements. The distortion is due to both amplitude and phase imperfections of the frequency response of the system within its bandwidth, as well as a limited bandwidth.

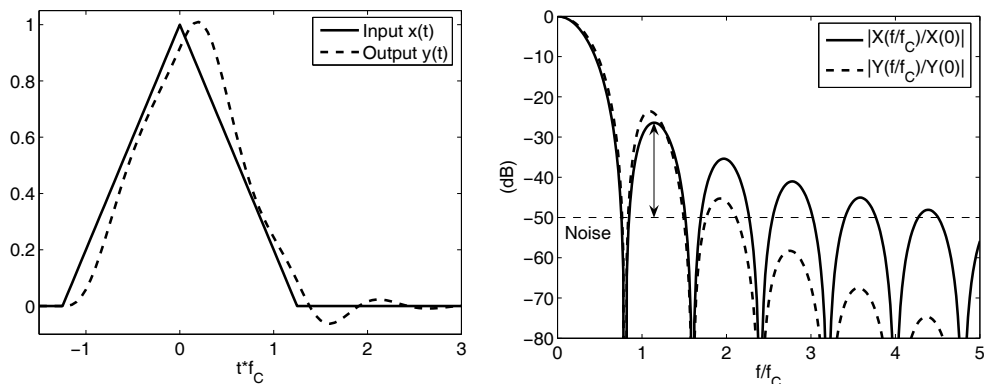


Fig. 2. Input and output signal of the measurement system (left) and magnitudes of their spectra (right). The arrow (right) indicates the signal-to-noise ratio ( $S/N$ ) of the input signal.

### 3.2 Dynamic correction

Correction of measured signals using knowledge of the measurement system (Pintelon et al., 1990; Hessling, 2010a) is practiced in many fields of science and engineering. Surprisingly, dynamic correction is not yet generally offered in the context of calibrations, despite that static corrections in principle are required (ISO GUM, 1993). Dynamic correction will here refer to reduction of all kinds of dynamic imperfections of the measurement. The digital correction filter essentially propagates measured signals backwards through a mathematical model of the system to their physical origin. Backwards propagation can be viewed as either an inverse or reversed propagation. Not surprisingly, reversed filtering is sometimes useful when realizing correction filters (Hessling, 2008a).

Correction requires an estimate of the inverse model of the measurement. In the time domain, it is a fairly complex operation to find the inverse differential equation. For a model parameterized in poles and zeros of a transfer function it is trivial. The inverse is then found by exchanging poles and zeros. A pole (zero) of the measurement system is then eliminated or *annihilated* with its 'conjugate' zero (pole) of the correction filter.

A generic and unavoidable problem for all methods of dynamic correction is due to the finite bandwidth of the measurement system. The bandwidth of the system and the level of measurement noise set a definite limit to which extent any signal may be corrected. The high frequency amplification of the inverse system is virtually without bound. Therefore, some kind of low-pass 'noise' filters must always be included in a correction. These reduce the total gain and hence the level of noise to a predefined acceptable level. Incidentally, if the sampling rate is low enough, the bandwidth set by the Nyquist frequency may be sufficient to limit the gain of the correction filter. The noise filter is preferably chosen 'optimal' to balance measurement error and noise in the most relevant way. To determine the degree of optimality requires a measure of the error, or the deviation between the corrected signal and the input signal of the measurement system. The time delay and the dynamic error are usually distinguished as different causes for deviations between signals (study Fig. 2, left). A unique definition of the time delay is therefore also required (Hessling, 2006). Since the error is different for different measured signals, so is also the optimal correction.

When dynamic correction fails it is usually either due to neglect of noise amplification, or insufficient model quality. On one hand, the required model quality may be underestimated. A model with almost perfect match of only the amplitude  $|H(i\omega)|$  of the frequency response may result in a 'correction' which *increases* the error! The phase  $\arg H(i\omega)$  is equally important as the magnitude (Ekstrom, 1972; Hessling, 2006): A correction applied with the wrong sign doubles instead of eliminates the error. On the other hand, the required model quality should not be overestimated. As long as the error is mainly due to bandwidth limitations, the model quality within the band is irrelevant. The best strategy is then to optimize the noise filter or regularization technique to be able to dig up the last piece of high frequency information from the measured signal (Hale & Dienstfrey, 2010).

The proposed pragmatic design (Hessling, 2008a) inspired by Wiener de-convolution (Wiener, 1949) will here be applied for determining the noise filter. To develop the method further, the noise filter will be determined for the actual input signal (Fig. 2). The correction filter is then not only *applied* to but also uniquely *synthesized* for every measured signal. The proposed optimal noise filter has a cross-over frequency  $f_N$  determined from the frequency

where the system amplification has decayed to the inverse of the signal-to-noise ratio ( $S/N$ ). The  $S/N$ -ratio oscillates for the triangular input signal. To find the desired cross-over it is thus necessary to estimate the envelope of the  $S/N$ -ratio, as shown in Fig. 3 (left) below. A property of the noise filter which is equally important as the cross-over is the asymptotic fall-off rate in the frequency domain (Hessling, 2006). The proposed noise filter is suggested to be applied symmetrically in both directions of time to cancel its phase. In that case, the fall-off rate of the noise filter and the measurement system should be the same. The fall-off rates of the correction filter with the noise filter applied twice and the measurement system are then the same. For the transducer, the noise filter should be of second order. Other details of the amplitude fall-off were ignored, as they are beyond reach for optimal correction in practice.

The prototype for correction was constructed by annihilating the poles of the model (Eq. 11) with zeros. This CT prototype was then sampled to DT using the simple exponential mapping (section 2.2). The poles and zeros of the correction filter are shown in Fig. 5 (top left). The impulse response (Fig. 5, bottom left) of the correction filter is non-causal since time-reversed noise filtering was adopted. The correction was carried out by filtering the output signal of the measurement system to find the corrected signal  $x_C$  in Fig. 3 (right).

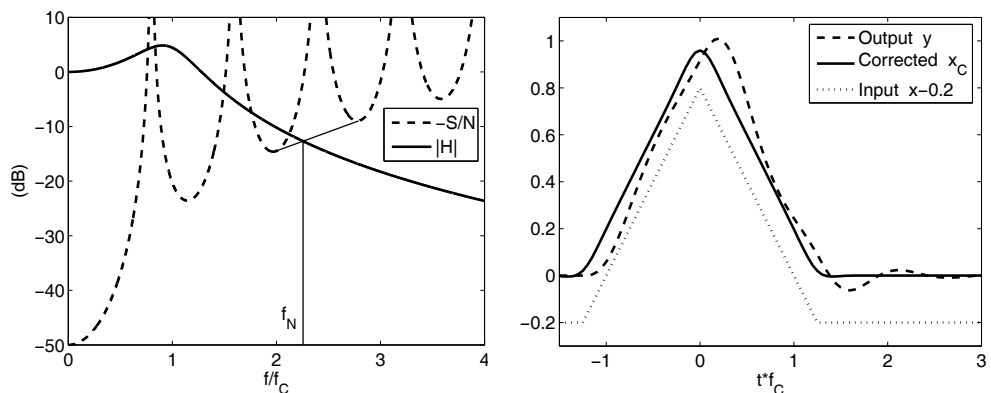


Fig. 3. Left: Signal to noise ratio ( $S/N$ ) for the input signal (Fig. 2) and amplification  $|H|$  of the measurement system, for determining the cut-off frequency  $f_N$  of the noise filter. Right: The output and the corrected output. The input signal is indicated (displaced for clarity).

### 3.3 Measurement uncertainty

The primary indicator of measurement quality is measurement uncertainty. It is usually expressed as a confidence interval for the measurement result. How to find the confidence interval from a probability density function (pdf) of the uncertain parameters that influence the quantity of interest is suggested in the Guide to the Expression of Uncertainty (ISO GUM, 1993). It is formulated for static measurements with a time-independent measurement equation. The dynamic measurements of interest here is beyond its original scope. Nevertheless, the guide is based on a standard perturbation analysis of first order which may be generalized to dynamic conditions. The instantaneous analysis is then

translated into filtering operations. The uncertainty of the parameters of the dynamic model and the measurement noise contribute to the dynamic measurement uncertainty. Only propagation of model uncertainty will be discussed here.

The linearity of a measurement system is a common source of misunderstanding. Any dynamic system  $h$  may be linear-in-response (LR), or linear-in-parameters (LP). LR does *not* imply that the output signal is proportional to the input signal. Instead it means that the response to a sum of signals  $y_1, y_2$  equals the sum of the responses of the signals, or  $h(\alpha y_1 + \beta y_2, q) = \alpha \cdot h(y_1, q) + \beta \cdot h(y_2, q)$ , for all  $\alpha, \beta$ . Analogously, a model LP would imply that  $h(y, \alpha q_1 + \beta q_2) = \alpha \cdot h(y, q_1) + \beta \cdot h(y, q_2)$ . A model  $h$  equal to a sum of LP models  $h_k$ ,  $h = \sum h_k$ , would then *not* be classified LP. Nevertheless, such models are normally considered LP as they are linear expansions. Therefore, any model that can be expressed as a sum of LP models will be considered LP.

To be a useful measurement system we normally require high linearity in response. Conventional linear digital filtering requires LR. A lot of effort is therefore made by manufacturers to fulfill this expectation and by calibrating parties to verify it. LR is a physical property of the system completely beyond control for the user, as well as the calibrator. In contrast, LP is determined by the model, which is partly *chosen* with the parameterization. It is for instance possible to exchange non-linearity in zeros with linearity in residues (section 3.1.1).

The non-linear propagation of measurement uncertainty by means of linear digital filtering in section 3.3.2 refers to measurement systems non-linear-in-parameters but linear-in-response. The presented method is an alternative to the non-degenerate unscented method (Hessling et. al., 2010b). At present there is no other published or established and consistent method used in calibrations for this type of non-linear propagation of measurement uncertainty, beyond inefficient Monte-Carlo simulations. For linear propagation of dynamic measurement uncertainty with digital filters, there is only one original publication (Hessling, 2009). In this reference, a complete description of estimation of measurement uncertainty is given.

### 3.3.1 Linear propagation using sensitivities

The established calculation of uncertainty (ISO GUM, 1993) follows the standard procedure of first order perturbation analysis adopted in most fields of science and engineering. Consistent application of the guide is strictly limited to linearization of the model equation (Hessling et. al., 2010b). Here, the analysis translates into linearization of the transfer function or impulse response in uncertain parameters. The derivation will closely follow a recent presentation (Hessling, 2010a). For correction of the mechanical transducer,

$$\delta H^{-1}(s) \approx \delta K \frac{\partial H^{-1}}{\partial K} + \delta p \frac{\partial H^{-1}}{\partial p} + \delta p^* \frac{\partial H^{-1}}{\partial p^*}. \quad (12)$$

The pole pair  $p, p^*$  of the original measurement system (section 3.1.1) is here a pair of zeros of the CT prototype  $H^{-1}$  of correction (section 3.2). The variations  $\delta p, \delta p^*$  are completely

correlated. Rather than modeling this correlation it is simpler to change variables. Evaluating the derivatives (Hessling, 2009),

$$\delta H^{-1}H(s) \approx E_K \frac{\delta K}{K} + E_p^{(22)}(s)\rho_1 + E_p^{(12)}(s)\rho_2,$$

$$E_K = -1, \quad E_p^{(m2)}(s) = \frac{2(-s/|p|)^m}{(p/|p| - s/|p|)(|p/|p| - s/|p|)}, \quad \rho_n = \frac{\delta p}{|p|} \cdot \left(\frac{p}{|p|}\right)^n. \tag{13}$$

If the dynamic sensitivity systems  $E_K, E_p^{(22)}(s), E_p^{(12)}(s)$  operate on the corrected signal  $x_c(t)$  it will result in three time-dependent sensitivity signals  $\xi_K(t), \xi_p^{(22)}(t), \xi_p^{(12)}(t)$  describing the sensitivity to the stochastic quantities  $\delta K/K, \rho_1, \rho_2$ . The latter quantities are written as vector scalar products or projections in the complex s-plane between the relative fluctuation  $\rho \equiv \delta p/|p|$  and powers of the normalized pole vector  $p/|p|$ , as illustrated in Fig. 4.

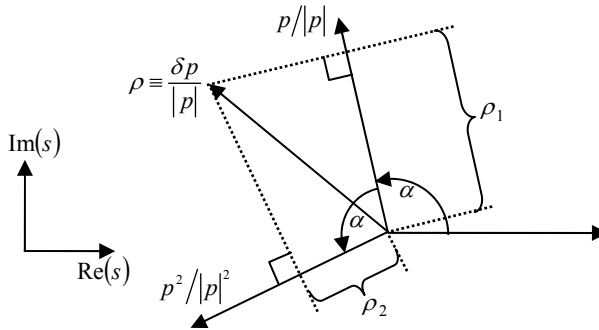


Fig. 4. Illustration of the relative variation  $\rho$  and associated projections  $\rho_1, \rho_2$  in the s-plane.

If the sensitivity signals  $\xi_K(t), \xi_p^{(22)}(t), \xi_p^{(12)}(t)$  are organized in rows of a  $3 \times m$  matrix  $\xi$ , the variation of the correction will be given by  $\chi = \xi^T \varphi, \varphi \equiv [\delta K/K \quad \rho_1 \quad \rho_2]^T$ . The auto-correlation function of the signal  $\chi$  resulting from the uncertainty of the model is found by squaring and calculating the statistical expectation  $\langle \cdot \rangle$  over the variations of the parameters,

$$\langle \chi \chi^T \rangle = \xi^T \langle \varphi \varphi^T \rangle \xi = \xi^T \text{cov}(K, \rho_1, \rho_2) \xi. \tag{14}$$

The matrix  $\langle \varphi \varphi^T \rangle$  of expectation values of squared parameter variations is usually referred to as the covariance matrix  $\text{cov}(K, \rho_1, \rho_2)$ . In Table 1 it was given in the parameters  $K, \text{Re}(p), \text{Im}(p)$ . In Table 2 it is translated to parameters  $K, \rho_1, \rho_2$  with a linear but non-unitary transformation  $T$  ( $TT^T \neq 1$ ) (Hessling, 2009),

$\text{cov}(K, \rho_1, \rho_2) = T \text{cov}(K, \text{Re}(p), \text{Im}(p)) T^T = 10^{-4} \begin{pmatrix} 0.50^2 & 0 & 0 \\ 0 & 1.70^2 & -1.68^2 \\ 0 & -1.68^2 & 1.83^2 \end{pmatrix}$
$\begin{pmatrix} K \\ \rho_1 \\ \rho_2 \end{pmatrix} = T \begin{pmatrix} K \\ p_R \\ p_I \end{pmatrix}, \quad T = \begin{pmatrix} 1 & 0 & 0 \\ 0 & p_R/ p  & p_I/ p  \\ 0 & p_R^2/ p ^2 - p_I^2/ p ^2 & 2p_I p_R/ p ^2 \end{pmatrix}, \quad \begin{matrix} p_R \equiv \text{Re}(p) \\ p_I \equiv \text{Im}(p) \end{matrix}$

Table 2. Covariance matrix for the static amplification and the two projections,  $(K, \rho_1, \rho_2)$ , and transformation matrix  $T$ . The covariance  $\text{cov}(K, \text{Re}(p), \text{Im}(p))$  is given in Table 1.

The measurement uncertainty is given by the *half-width*  $x_p$  of the confidence interval of the measurement. This width can be calculated as the standard deviation at each time instant, multiplied by an estimated coverage factor  $k_p$  (ISO GUM, 1993). This coverage factor is difficult to determine accurately for dynamic measurements, since the type of distribution varies with time. The standard deviation is obtained as the square root of the variance, i.e. the square root of the auto-correlation for zero lag,

$$u = k_p \cdot \sqrt{\text{diag}(\langle \chi \chi^T \rangle)} = k_p \cdot \sqrt{\text{diag}(\xi^T \text{cov}(K, \rho_1, \rho_2) \xi)}. \tag{15}$$

The sensitivity signals  $\xi$  can be calculated with digital filtering. *Sensitivity filters* are found by sampling the CT sensitivity systems  $E_K, E_p^{(22)}(s), E_p^{(12)}(s)$ . The noise filter is a necessity rather than a part of the actual correction and gives rise to a systematic error. The uncertainty of the noise filtering is thus the same as the uncertainty of this systematic error. That is of no interest without an accurate estimate of the systematic error. Estimating this error is very difficult since much of the required information is unconditionally lost in the measurement due to bandwidth limitations. No method has been presented other than a very rough universal conservative estimate (Hessling, 2006). The uncertainty of the error is much less than the accuracy of this estimate and therefore completely irrelevant.

The gain of the sensitivity filters is bounded at all frequencies and no additional noise filters are required. The sensitivity filters differ from the correction filter in numerous ways: As the complexity of the model increases, the types of sensitivity filter remain but their number increases. There are only three types of sensitivity filters, one for real-valued and the same pair for complex-valued poles and zeros. For the transducer, the correction filter and the two sensitivity filters were sampled with the same exponential mapping (section 2.2). The resulting impulse responses and z-plane plots of all filters are shown in Fig. 5.

Filtering the corrected signal with the sensitivity filters  $E_K, E_p^{(22)}(z), E_p^{(12)}(z)$  resulted in the sensitivities  $\xi_K(t), \xi_p^{(22)}(t), \xi_p^{(12)}(t)$  in Fig. 6 (left). The time-dependent half-width of the confidence interval for the correction in Fig. 6 (right) was then found from Eq. 15, using the covariance matrix in Table 2 and  $k_p = 2$  for an assumed normal distributed correction.

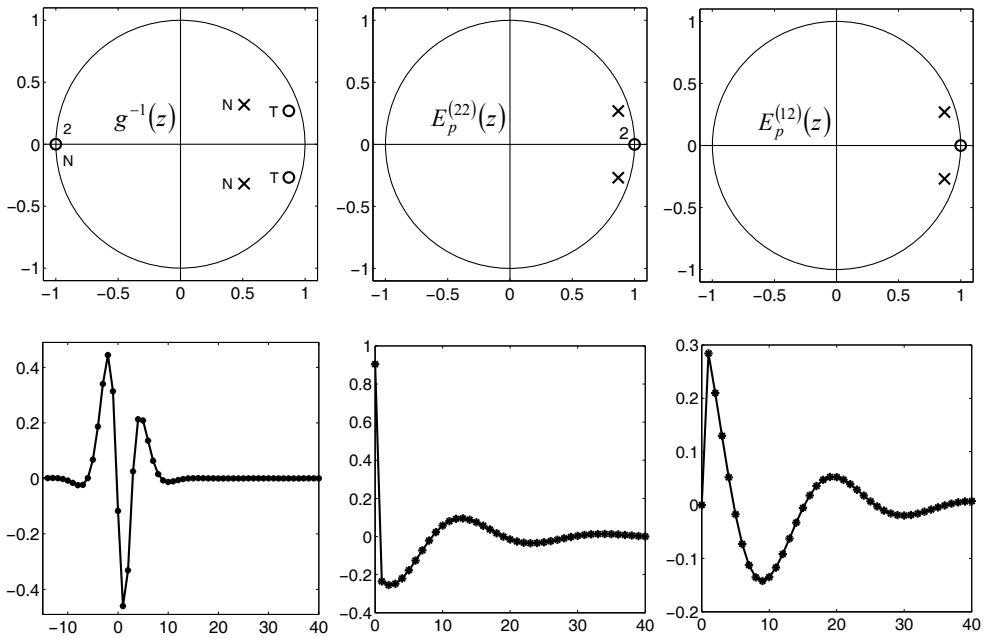


Fig. 5. Poles (x) and zeros (o) (top) and impulse responses (bottom) of the correction  $g^{-1}(z)$  (left) and digital sensitivity filters  $E_p^{(22)}(z)$  (middle) and  $E_p^{(12)}(z)$  (right) for the two projections  $\rho_1$  and  $\rho_2$ , respectively.

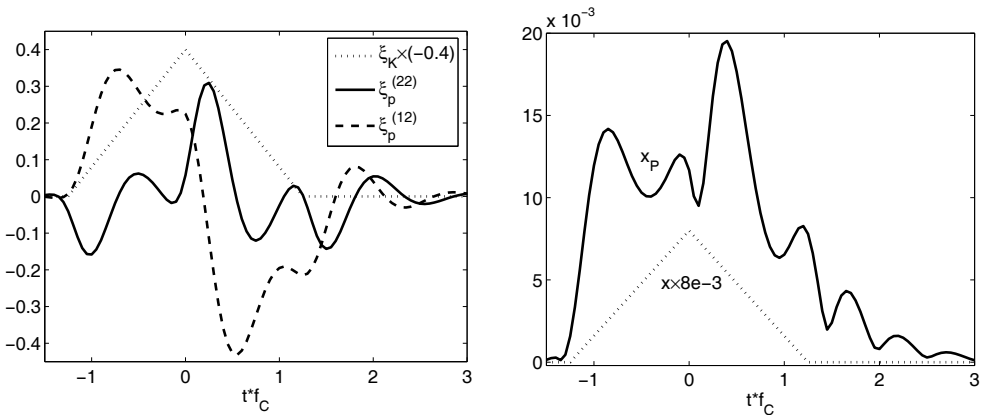


Fig. 6. Left: Sensitivity signals  $\xi$  for the amplification  $K$  and the two pole projections  $\rho_1, \rho_2$ , obtained by digital filtering of the corrected output shown in Fig. 3 (right). Right: Resulting confidence interval half-width  $x_p$ . For comparison, the rescaled input signal is shown (dotted).

### 3.3.2 Non-linear propagation utilizing unscented binary sampling

The uncertainty of the correction can be estimated by simulating a representative set or ensemble of different corrections of the same measured signal. The probability density function (pdf) of the parameters is then sampled to form a *finite* number of 'typical' sets of parameters: The multivariate pdf  $f(\{q_k\})$  for all parameters  $\{q_k\}$  is substituted with an ensemble of  $m$  sets of  $n$  samples  $\{\hat{q}_k^{(v)}\}$ , where  $v=1,2,\dots,m$  denotes the different members of the ensemble and  $k=1,2,\dots,n$  the different parameters of the model. To be most relevant, these sets should preserve as many statistical moments as possible. Expressed in deviations  $\delta\hat{q}_k^{(v)} \equiv \hat{q}_k^{(v)} - \langle \hat{q}_k^{(v)} \rangle$  from the first moment,

$$\begin{aligned}
 0 = \langle \delta q_i \rangle &= \int \delta q_i f(\{q_k\}) dq_1 dq_2 \dots dq_n \hat{=} \frac{1}{m} \sum_{v=1}^m \delta \hat{q}_i^{(v)} \\
 \langle \delta q_i \delta q_j \rangle &= \int \delta q_i \delta q_j f(\{q_k\}) dq_1 dq_2 \dots dq_n \hat{=} \frac{1}{m} \sum_{v=1}^m \delta \hat{q}_i^{(v)} \delta \hat{q}_j^{(v)} \\
 \langle \delta q_i \delta q_j \delta q_k \rangle &= \dots \hat{=} \frac{1}{m} \sum_{v=1}^m \delta \hat{q}_i^{(v)} \delta \hat{q}_j^{(v)} \delta \hat{q}_k^{(v)} \\
 \vdots &= \dots \hat{=} \dots
 \end{aligned} \tag{16}$$

The *sampling of the pdf* is indicated by  $\hat{=}$ . In contrast to signals and systems, pdfs are not physical and not observable. That makes sampling of pdfs even less evident than sampling of systems (section 2.2). Only a few of many possible methods have so far been proposed.

Perhaps the most common way to generate an ensemble  $\{\delta\hat{q}_k^{(v)}\}$  is to employ random generators with the same statistical properties as the pdf to be sampled. With a sufficiently large ensemble, typically  $m \sim 10^6$ , all relevant moments of pdfs of *independent* parameters may be accurately represented. This random sampling technique is the well known Monte Carlo (MC) simulation method (Metropolis, 1949; Rubenstein, 2007). It has been extensively used for many decades in virtually all fields of science where statistical models are used. The efficiency of MC is low: Its outstanding simplicity of application is paid with an equally outstanding excess of numerical simulations. It thus relies heavily upon technological achievements in computing and synthesis of good random generators. Modeling of dependent parameters provides a challenge though. With a linear change of variables, ensembles with any second moment or covariance may be generated from independent generators. It is generally difficult to include any higher order moment in the MC method in any other way than directly construct random generators with relevant dependences. Another constraint is that the models must not be numerically demanding as the number of simulations is just as large as the size of the ensemble ( $m$ ). For dynamic measurements this is an essential limitation since every realized measurement requires a full dynamic simulation of a differential equation over the entire time epoch. For a calibration service the limitation is even stronger as the computers for evaluation belongs to the customer and not the calibrator. A fairly low computing power must therefore be allowed. There are thus many reasons to search for more effective sampling strategies.

An alternative to random sampling is to construct the set  $\{\delta\hat{q}_k^{(v)}\}$  from the given statistical moments (Eq. 16) with a *deterministic* method. The first versions of this type of *unscented*

sampling techniques appeared around 15 years ago and was proposed by Simon Julier and Jeffrey Uhlmann (Julier, 1995) for use in Kalman filters (Julier, 2004). The name unscented means without smell or bias and refers to the fact that *no* approximation of the deterministic model is made. The number of realizations is much lower and the efficiency correspondingly higher for unscented than for random sampling. The unavoidable cost is a lower statistical accuracy as fewer moments are correctly described. The realized vectors of parameters  $\{\hat{q}_1^{(v)} \hat{q}_2^{(v)} \dots \hat{q}_n^{(v)}\}$  were called *sigma-points* since they were constructed to correctly reproduce the second moments. The required *minimum* number of such points, or samples depends on how many moments one wants to correctly describe. The *actual* number of samples is often larger and depends on the sampling strategy. There is no general approach for deterministic sampling of pdf corresponding to the use of random generators for random sampling. The class of unscented sampling techniques is very large. It is all up to your creativity to find a method which reproduce as many moments as possible with an acceptable number of sigma-points. For correct reproduction of the first and second moment, the simplex set of sigma-points (Julier, 2004, App. III) utilizes the minimum number of  $n+1$  samples while the standard unscented Kalman filter use  $2n$  samples (Simon, 2006). The minimum number of samples is given by the number of degrees-of-freedom (NDOF). For the first and second moment,  $NDOF=1+n$ . The sampling method that will be presented here is close to the standard UKF, apart from a few important differences:

- The amplification of the standard deviation with  $\sqrt{n} > 1$  in the standard UKF (see below) is strongly undesirable since parameters may be sampled outside their region of possible variation, which is prohibited. For instance, poles must remain in the left hand side of the s-plane to preserve stability. The factor  $\sqrt{n}$  may violate such critical physical constraints.
- The confidence interval of the measurement is of primary interest in calibrations, rather than the covariance as in the UKF. For non-linear propagation of uncertainty it is crucial to expand the sampled parameters to the desired confidence level, and not the result of the simulation. Expanded sigma-points will be denoted *lambda-points*. This expansion makes the first aspect even more critical.

The standard UKF samples sigma-points by calculating a square root of the covariance matrix. A square root is easily found if the covariance matrix first is transformed to become diagonal. To simplify notation, let  $q = [q_1 \ q_2 \ \dots \ q_n]^T$ . It is a widely practiced standard method (Matlab, m-function 'eig') to determine a unitary transformation  $U$ , which makes the covariance matrix diagonal,

$$\text{cov}(U\delta q) = U \text{cov}(q)U^T = \text{diag}(\sigma_1^2 \ \sigma_2^2 \ \dots \ \sigma_n^2), \quad UU^T = U^T U = 1. \quad (17)$$

The first moments (Eq. 16) will vanish if the lambda-points  $\hat{q}^{(v)} \rightarrow \lambda^{(v,s)}$  are sampled symmetrically around the mean  $\langle q \rangle$ . Expressing the sampled variations  $\delta \hat{q}^{(v)}$  in the diagonal basis and expanding with coverage factors  $k_p^{(v)}$ ,

$$\lambda^{(v,s)} = \langle q \rangle + s \cdot k_p^{(v)} U^T \delta \hat{q}^{(v)}, \quad v=1,2,\dots,m/2, \quad s=\pm. \quad (18)$$

The column vectors  $\delta q^{(v)}$  of variations are for convenience collected into columns of a matrix  $\Delta$ . The condition to reproduce the second moment in Eq. 16 then reads,

$$\text{diag}(\sigma_1^2 \ \sigma_2^2 \ \dots \ \sigma_n^2) = \frac{2}{m} \Delta \Delta^T. \tag{19}$$

Clearly,  $\Delta = \sqrt{m/2} \cdot \text{diag}(\sigma_1 \ \sigma_2 \ \dots \ \sigma_n)$  ( $m = 2n$ ) is a valid but as will be discussed, not a unique solution. Except for the unitary transformation, that corresponds to the standard UKF (Simon, 2006, chapter 14.2). The factor  $\sqrt{m/2}$  may result in prohibited lambda-points and appeared as a consequence of normalization. This square root is by no means unique: Any ‘half’-unitary<sup>1</sup> transformation  $\tilde{\Delta} \equiv \Delta V, VV^T = 1$  yields an equally acceptable square root matrix since  $\tilde{\Delta} \tilde{\Delta}^T \equiv \Delta V V^T \Delta^T = \Delta \Delta^T$ . This degree of freedom will be utilized to eliminate the factor  $\sqrt{m/2}$ . Note that  $VV^T = 1$  does not imply that  $V$  must be a square matrix, or  $m = 2n$ . To arrive at an arbitrary covariance matrix though, the rank of  $V$  must be at least the same as for  $\text{cov}(U\delta q)$ , or  $m \geq 2n$ . Since the ‘excitation’ of the different parameters is controlled by the matrix  $V$  it will be called the *excitation matrix*. The lambda-points are given by,

$$\lambda^{(v,s)} = \langle q \rangle + s \cdot k_p^{(v)} U^T \sqrt{\text{cov}(q)} U^T U \Psi^{(v)}, \quad \Psi = (\Psi^{(1)} \ \Psi^{(2)} \ \dots \ \Psi^{(m/2)}) \equiv \sqrt{m/2} U^T V. \tag{20}$$

Here,  $\Psi^{(v)}$  is column  $v$  of the scaled excitation matrix, expressed in the original basis of correlated coordinates  $q$ . The main purpose of applying the unitary transformation or rotation  $U$  as well as using the excitation matrix  $V$  is to find physically allowed lambda-points in a simple way.

After the pdf has been sampled into lambda-points  $(\lambda)$ , the confidence interval  $[x_C(t) - x_P(t), x_C(t) + x_P(t)]$  of the corrected signal  $\hat{x}(t)$  is evaluated as,

$$\begin{aligned} x_C(t) &= \langle \hat{x}(\lambda, t) \rangle_\lambda, \quad \hat{x}(\lambda, t) = y(t) * g^{-1}(\lambda, t), \quad \langle f \rangle_\lambda \equiv \frac{1}{m} \sum_{v=1}^m f(\lambda^{(v)}) \\ x_P(t) &= \sqrt{\langle [\hat{x}(\lambda, t) - x_C(t)]^2 \rangle_\lambda} \end{aligned} \tag{21}$$

The impulse response of the digital correction filter is here denoted  $g^{-1}(\lambda, t)$  and  $y$  is the measured signal, while the filtering operation is described by the convolution  $*$  (section 3.2). The auto-correlation function of the measurement may be similarly obtained from the associated sigma-points (let  $k_p^{(v)} \rightarrow 1$  and  $\lambda \rightarrow \sigma$  in Eqs. 20-21),

$$\langle \delta x(t) \delta x(t - \tau) \rangle = \langle [\hat{x}(\sigma, t) - x_C(t)] \cdot [\hat{x}(\sigma, t - \tau) - x_C(t - \tau)] \rangle_\sigma. \tag{22}$$

---

<sup>1</sup> The matrix is not unitary since that also requires  $V^T V = 1$ .

As a matter of fact, it is simple to evaluate all statistical moments of the correction,

$$\langle \delta x(t_1) \delta x(t_2) \cdots \delta x(t_r) \rangle = \left\langle \prod_{k=1}^r [\hat{x}(\sigma, t_k) - x_c(t_k)] \right\rangle_{\sigma} . \quad (23)$$

Consistency however, requires at least as many moments of the sampled parameters to agree with the underlying pdf (Eq. 16). It is no coincidence that for propagating the covariance of the parameters to the correction, the mean and the covariance of the sampled parameters were correctly described. Thus, to propagate higher order moments the sampling strategy needs to be further improved.

The factor  $\sqrt{m/2}$  may be extinguished by exciting all uncertain parameters, i.e. filling all entries of  $V$  with elements of unit magnitude, but with different signs chosen to obtain orthogonal rows. This will lead to  $m = 2^n$  lambda-points instead of  $m = 2n$ . Since the lambda-points will represent all binary combinations, this sampling algorithm will be called the method of *unscented binary sampling* (Hessling, 2010c). All lambda-points will be allowed since the scaling factor  $\sqrt{m/2}$  will disappear with the normalization of  $V$ . The *combined* excitation of several parameters may nevertheless not be statistically allowed. This subtlety is not applicable within the current second moment approximation of sampling and can be ignored. The rapid increase in the number of lambda-points for large  $n$  is indeed a high price to pay. For dynamic measurements this is worth paying for as prohibited lambda-points may even result in unstable and/or un-physical simulations! In practice, the number of parameters is usually rather low. It may also be possible to remove a significant number of samples. The only requirements are that the rank of  $V$  is sufficient ( $m \geq 2n$ ), and that the half-unitary condition ( $VV^T = 1$ ) can be met.

For the mechanical transducer, there are three uncertain parameters, the amplification and the real and imaginary parts of the pole pair ( $\lambda = K, \text{Re}(p), \text{Im}(p)$ ). The full binary excitation matrix is for three parameters given by,

$$V = \frac{1}{2} \begin{pmatrix} 1 & -1 & 1 & -1 \\ 1 & 1 & -1 & -1 \\ 1 & 1 & 1 & 1 \end{pmatrix} . \quad (24)$$

Unscented binary sampling thus resulted in  $m = 2^3 = 8$  'binary' lambda-points, or digital correction filters illustrated in Fig. 7 (top left). Applying these filters to the measured signal yielded eight corrected signals, see Fig. 7 (top right). The statistical evaluation at every instant of time (Eq. 21) resulted in the confidence interval of the correction displayed in Fig. 7 (bottom). The coverage factors were assumed to be equal and represent normal distributed parameters ( $k_p = 2$ ).

The simplicity of unscented propagation is striking. The uncertainty of correction is found by filtering measured signals with a 'typical' set of correction filter(-s). An already implemented dynamic correction (Bruel&Kjaer, 2006) can thus easily be parallelized to also find its time-dependent uncertainty, which is unique for every measured signal.

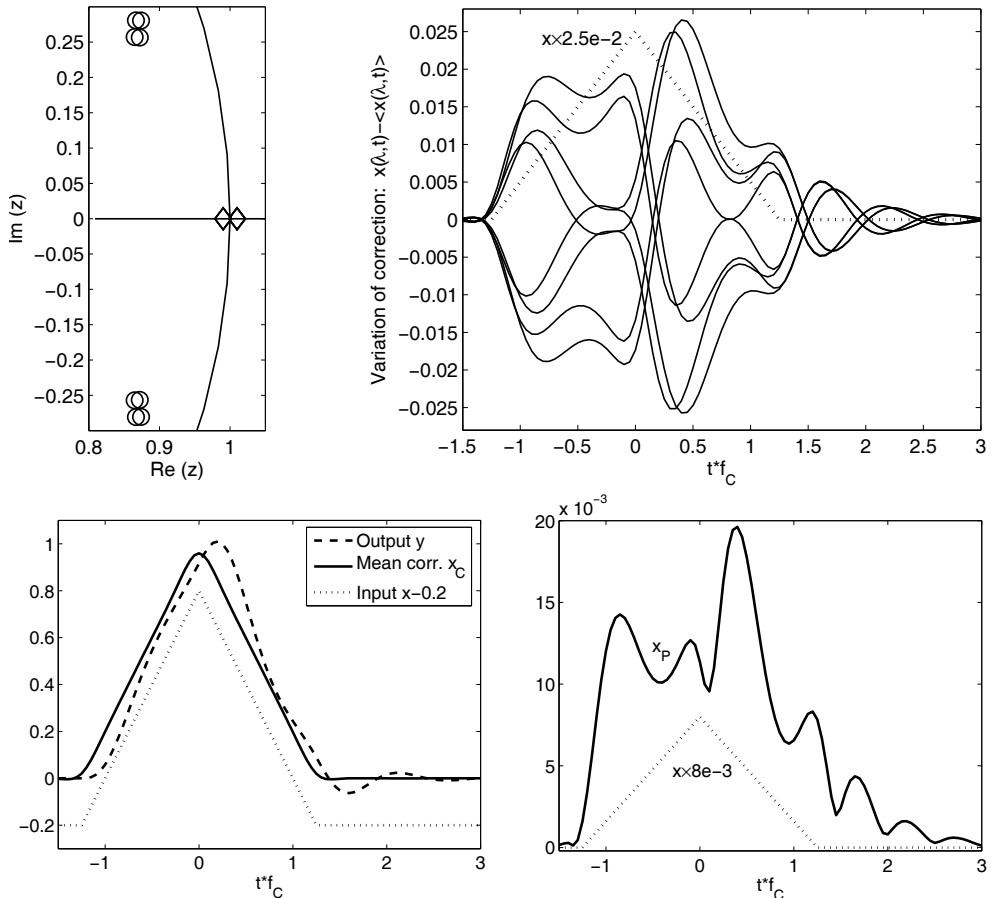


Fig. 7. Top left: Poles and zeros of the eight sampled digital correction filters, excluding the fixed noise filter. The static gains ( $\diamond$ ) are displayed on the real  $z$ -axis (close to  $z=1$ ). Top right: The variation of all corrections from their mean. Bottom: Center  $x_C$  (left) and half-width  $x_p$  (right) of the confidence interval for the correction. The (rescaled/displaced) input signal of the measurement system is shown (dotted) for comparison.

### 3.3.3 Comparison of methods

The two proposed methods in sections 3.3.1 and 3.3.2 for estimating the model uncertainty are equivalent and may be compared. The correct confidence interval is not known but can be estimated by means of computationally expensive random sampling or Monte Carlo simulations (Rubenstein, 2007). The lambda-points are then substituted with a much larger ensemble generated by random sampling. The errors of the estimated confidence interval of the correction were found to be different for the two methods, see Fig. 8.

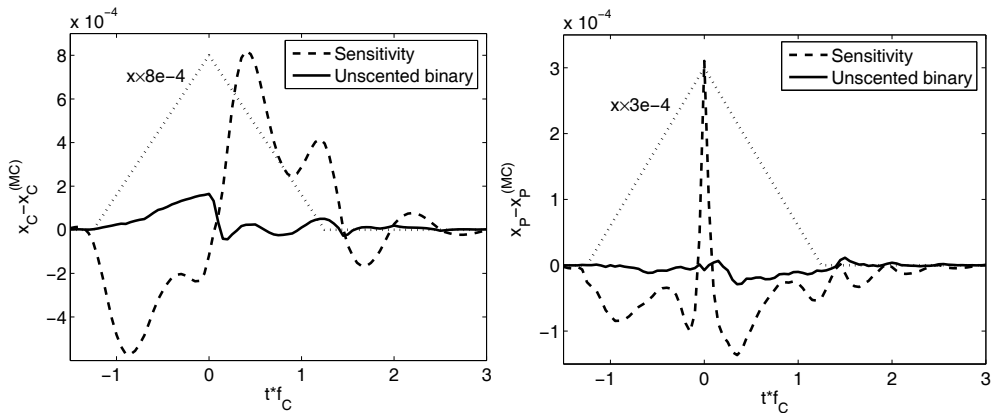


Fig. 8. The errors of the center  $x_C$  (left) and the half-width  $x_P$  (right) of the confidence interval of the correction, for the sensitivity analysis (section 3.3.1) and the method of unscented binary sampling (section 3.3.2). The errors are estimated with random sampling of  $10^6$  correction filters. For comparison, the rescaled input signal is shown (dotted).

The center (Fig. 8, left) as well as the width (Fig. 8, right) is best determined with the unscented binary method, in agreement with the performance of extended (based on sensitivity) and unscented Kalman filters (Julier, 2004). The errors of the sensitivity analysis are small which indicate minor non-linear effects. The half-width of the confidence interval, or measurement uncertainty changes much less ( $\leq 3e-4$ ) due to non-linear effects, than the center ( $\leq 8e-4$ ) of the interval. That is typical for non-linear propagation of uncertainty. Hence it is inconsistent to include non-linear contributions in the estimate of the measurement uncertainty but not in the estimate of the mean correction (Hessling, 2010b). The unscented method might be superior in performance but its simplicity is perhaps a greater advantage. The calculation of time-dependent sensitivities is also a source for making mistakes.

The unitary transformation  $U$  was here chosen (Eq. 17) to easily find *time-invariant* lambda-points, rather than to be optimal. An optimized choice is made in the unscented non-degenerate method (Hessling, 2010b). The *time-varying* lambda-points are then sampled in the direction of the time-dependent gradient (in the parameter space).

The estimation of mean correction and estimation of uncertainty with sensitivities were made with different methods. With unscented sampling these operations are synthesized jointly as different statistical moments. The symmetry implies that the analysis can be extended to higher moments to more accurately include parametric dependencies. However, that would require a sampling method which takes more moments into account (Eq. 16), as well as much more information of the stochastic dynamic model than is usually available.

## 4. Feature extraction

There are many examples of extracting dynamic information from measurements which qualify as 'feature extraction' and can be partly or completely realized with digital filters. A crucial aspect is to have a complete and robust specification of the feature to be extracted. The two selected examples here are related to the safety of traffic, road hump analysis and determination of road texture.

### 4.1 Road humps

Maintaining speed limits in the traffic is a global problem. Radar measurements of the speed and supervision by policemen are commonly used to enforce speed limits. A popular passive control measure is the 'sleeping policeman' or road hump (Engwall, 1979). Vehicles are intentionally excited in excess when passing the hump which is a modified usually elevated short (~3-20m) section of the road. Below the speed limit, road humps should provide a safe and comfortable passage, but also be gentle to the vehicle. Above the speed limit, the discomfort should increase rapidly to enforce a distinct speed reduction. With respect to the human reaction, there are two important features of all road humps, one positive and one negative: their efficiency and the risk of injury. The efficiency is central for any particular hump design (Hessling & Zhu, 2008c). The risk of injury is normally low for single passages, but for multiple daily passages it may be substantial. Especially for professional drivers of taxis and buses in towns with many road humps this may be a problem. What has been in focus and will be addressed here is the potential damage of the human lumbar spine.

The vibration pulses generated by vehicles travelling over rough surfaces such as road humps are believed to cause fatigue stresses in the lumbar spine. Modeling of the load on the human body is rather complex and is described in a recent international standard for evaluating the human exposure to whole-body vibrations (ISO 2631-5, 2004). It is based on non-linear digital filtering followed by statistical evaluation. The adverse health effects of prolonged exposure are condensed into an 'R'-dose. This dose is the feature to extract from every complex set of road hump passages. A typical driver uses different vehicles, follows different time tables and drive on different roads, from the first to the last working day. The dose is normalized to unity which is the threshold for a 'significant' risk of injury. The calculation of the dose consists of counting peak amplitudes and weighing with exponent six. This weighing models the accumulated fatigue stress of the lumbar spine.

The standard for whole body vibration (ISO 2631-5, 2004) addresses the propagation of vibrations from the seat pad of the driver seat to the spinal cord. The road hump problem is more complex. Geometric road hump profiles are translated into an excitation signal in time via the variable speed of the vehicles. For a fixed hump, the bandwidth of the road height signal increases with the speed – that is the fundamental principle of road humps. The vehicles may also be drastically different with respect to size as well as construction. For instance, the center-of-gravity is far away from the driver in buses but not in cars. This affects the response substantially (Hessling & Zhu, 2008c). The seats may also be different. Preferably, the vehicle as well as the seat response may be simulated with digital filters, just like the human response. The analysis of a particular road hump passage is then made with several digital filters, as shown in Fig. 9 below. The human lumbar spine filter and the vehicle filters are non-trivial and will be discussed below.

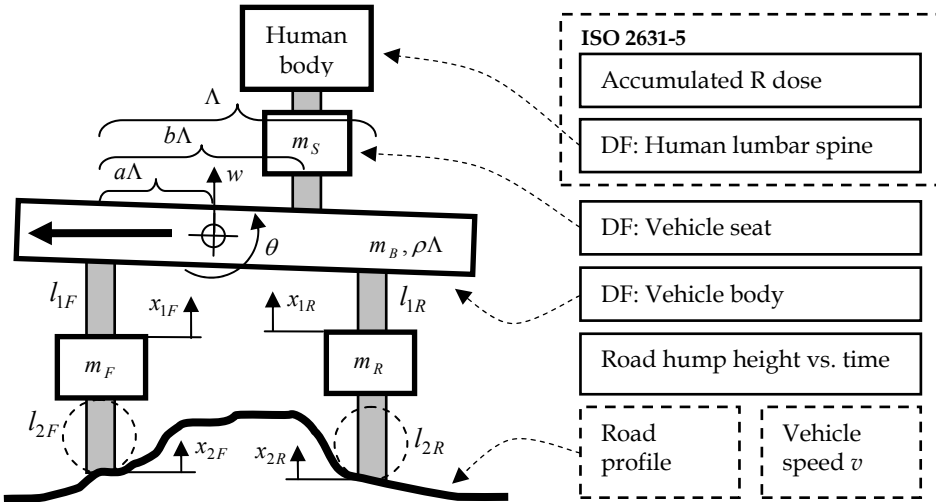


Fig. 9. The road hump response from the road, via the vehicle (moves to the left), to the human lumbar spine (left), is simulated with multiple digital filtering (DF) (right).

#### 4.1.1 Human lumbar spine filter

In the horizontal directions, the response of the lumbar spine is modeled with a linear second order resonant system with one degree of freedom, similar to the transducer in section 3.1.1. In the vertical direction, advanced non-linear filtering is applied. The predominant vertical motion will be discussed here. All details of the evaluation of the lumbar spine response are included in the standard (ISO 2631-5, 2004). Aspects of particular interest in the context of digital filtering will be highlighted here. The (output) vertical lumbar spine acceleration  $y(k)$  at time sample  $t_k = kT_s$  is calculated with a *recurrent neural network* (RNN) model from the (input) seat acceleration  $x(k)$  as,

$$y(k) = \sum_{j=1}^7 W_j u_j(k) + W_8 \tag{25a-b}$$

$$u_j(k) = \tanh \left[ \sum_{i=1}^4 w_{ji} y(k-i) + \sum_{i=5}^{12} w_{ji} x(k-i+4) + w_{j13} \right]$$

The constants  $w_{ji}, W_j$  are given in the standard, where also the derivation of this RNN is discussed (annex C). The RNN is a non-linear IIR filter. The output is a linear combination of neurons  $u_j(k)$  (Eq. 25b). If the neurons are viewed as input signals, the model is static and linear as only neurons at the same time instant ( $k$ ) as the output are weighted (Eq. 25a). Disregarding this weighing of neurons and considering  $x(k)$  as input and  $y(k)$  as output, the second sum in Eq. 25b corresponds to a FIR-filter while the first sum describes the recursion or feed-back of an IIR-filter. The tanh function provides the non-linearity which is individually tuned for each neuron by adjusting the constants  $w_{j13} \in [-0.96, 1.03]$ .

The small amplitude dynamic response of the lumbar spine can be understood by a linear approximation of the filter. If each neuron  $u_j$  is linearized around  $w_{j13}$ ,

$$\sum_{i=0}^4 a_i y(k-i) = \sum_{i=0}^8 b_i x(k-i) \tag{26}$$

$$a = [1 \quad -\alpha_1 \quad -\alpha_2 \quad -\alpha_3 \quad -\alpha_4], \quad \alpha_i \equiv \sum_{j=1}^7 W_j [1 - \tanh^2(w_{j13})] w_{ji}$$

$$b = [0 \quad \alpha_5 \quad \alpha_6 \quad \dots \quad \alpha_{12}]$$

The poles, zeros and the magnitude of the frequency response of this filter are shown in Fig. 10. The amplitude response is almost flat (-1.5 dB/octave, 10 Hz ≤ f ≤ 20 Hz) above the peak at 4.7 Hz generated by nearly cancelation of a pole and a zero pair.

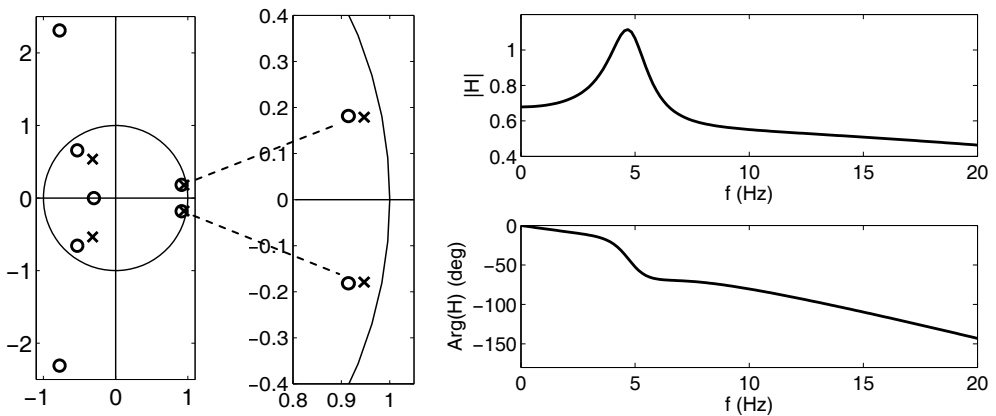


Fig. 10. All poles and zeros (left), the almost cancelling pole and zero pairs (middle) and the frequency response (right) of the linearized human lumbar spine filter.

The degree of non-linearity is different for different neurons, since their weights  $w_{j13}$  are different (Eq. 25). The onset of non-linear behavior in each neuron can be found by quadratic expansion,  $\tanh(a_0 + w) \approx \tanh(w) + a_0 \partial \tanh(w) + a_0^2 / 2 \cdot \partial^2 \tanh(w)$ , for a constant input acceleration  $a_0$ . The largest ratio between the quadratic and linear term is given by,

$$\max_j \left[ \frac{a_0 \partial^2 \tanh(w_{j13})}{2 \cdot \partial \tanh(w_{j13})} \right] = a_0 \cdot \max_j \left[ \left( H(0) \cdot \sum_{i=1}^4 w_{ji} + \sum_{i=5}^{12} w_{ji} \right) \tanh(w_{j13}) \right] \approx 0.02 \cdot a_0 \tag{27}$$

A significant non-linearity (≤ 20%) is expected for  $a_0 \geq 10 \text{ m/s}^2$ . Indeed, that is confirmed by the simulations in Fig. 11. The response of the lumbar spine filter is linear for accelerations  $a \leq 1 \text{ m/s}^2$  and static for pulse widths  $\tau \gg 1/f_C = 0.2 \text{ s}$ .

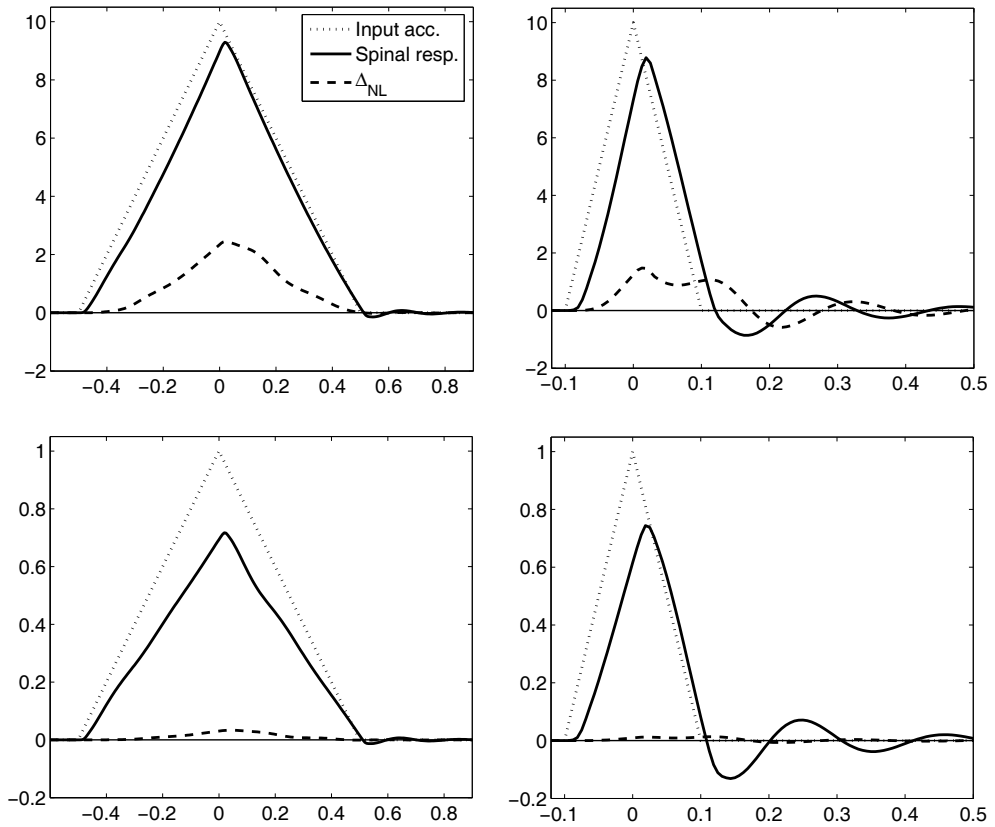


Fig. 11. Lumbar spine response and its difference to linearized response  $\Delta_{NL}$ , for various pulse acceleration amplitudes  $A$  and widths  $T$ :  $A = 10 m/s^2$  (top),  $A = 1 m/s^2$  (bottom),  $T = 1 s$  (left), and  $T = 0.2 s$  (right). The units are  $m/s^2$  (vertical) and  $s$  (horizontal).

#### 4.1.2 Vehicle filters

A vehicle is a dynamic system which responds to the road hump signal, similarly to how a measurement system responds to its input signal. A vehicle is a composed mechanical system. It may be approximated with a lumped linear system with solid masses ( $m$ ) and spring ( $l = k$ ) and damping elements ( $l = c$ ) (Hessling et. al., 2008c), similarly to a recent model of material testing machines (Hessling, 2008b). A two axes vehicle is modeled in Fig. 9 (left). The front ( $x_{2F}$ ) and rear ( $x_{2R}$ ) coordinates are the two related input signals describing height,  $x_{2R}(t) = x_{2F}(t - \Lambda/v)$ , where  $\Lambda$  is the distance between the axes and  $v$  is the speed. The translation  $w$  and scaled rotation  $\Lambda\theta$  of the vehicle are the two outputs. The transfer function is thus a  $2 \times 2$  matrix. The topology of the model can be expressed by a symmetric matrix,

$$L = \begin{pmatrix} -l_{1F} - l_{1R} & a l_{1F} - (1-a) l_{1R} & l_{1F} & l_{1R} \\ a l_{1F} - (1-a) l_{1R} & -a^2 l_{1F} + (1-a)^2 l_{1R} & -a l_{1F} & (1-a) l_{1R} \\ l_{1F} & -a l_{1F} & -l_{1F} - l_{2F} & 0 \\ l_{1R} & (1-a) l_{1R} & 0 & -l_{1R} - l_{2R} \end{pmatrix}. \tag{28}$$

When used for the spring (damping) constants  $l_n = k_n$  ( $l_n = c_n$ ), the matrix will be denoted  $K$  ( $C$ ). The dynamic equations are given by Newton’s force and torque laws,

$$\sum_n f_{kn} = m_k \partial_t^2 x_k, \quad \sum_n \frac{\mu_n}{\Lambda} = \rho^2 m_B \partial_t^2 (\Lambda \theta), \tag{29}$$

where  $\partial_t$  is the time-derivative while  $f_{kn}$  and  $\mu_n$  represent the  $n$ -th force and torque, respectively, and  $\rho \Lambda$  is the radius of gyration. For a contraction  $\Delta x$ , the spring force is  $f = -k \Delta x$  and the damping force  $f = -c \partial_t \Delta x$ . The topology matrix in Eq. 28 results from Eq. 29 with a specific choice of state-space variables  $u \equiv (u_1 \ u_2 \ \dots \ u_8)^T$ ,

$$\begin{aligned} (u_1 \ u_2 \ u_3 \ u_4) &\equiv (w \ \Lambda \theta \ x_{1F} \ x_{1R}) \\ u_{k+d} &\equiv \partial_t u_k, \quad k=1,2,3,4 \end{aligned} \tag{30}$$

The state-space equation will be given in the topology matrix  $L \rightarrow K, C$ ,

$$\begin{aligned} \begin{pmatrix} 1 & 0 \\ 0 & \hat{M} \end{pmatrix} \partial_t u &= \begin{pmatrix} 0 & 1 \\ K & C \end{pmatrix} u + E \begin{pmatrix} x_{2F} \\ x_{2R} \end{pmatrix} \\ \hat{M} &= \text{diag}(M \ \rho^2 m_B \ m_F \ m_R) \\ E &= \begin{pmatrix} 0 & \dots & 0 & k_{2F} + c_{2F} \partial_t & 0 \\ 0 & \dots & 0 & 0 & k_{2R} + c_{2R} \partial_t \end{pmatrix}^T \end{aligned} \tag{31}$$

The measurement equation relates the seat coordinate (Fig. 9) to the state-space variables,

$$y = (1 \ (b-a) \ 0 \ \dots \ 0) u \equiv P u. \tag{32}$$

The transfer function from the road hump signal, or front wheel coordinate  $x_{2F}(t)$  is found by applying the La-place transform to the state-space equation (Eq. 31) as in section 2.3,

$$H(s) = P \left[ s - \begin{pmatrix} 0 & 1 \\ \hat{M}^{-1} K & \hat{M}^{-1} C \end{pmatrix} \right]^{-1} E(s) \begin{pmatrix} 1 \\ e^{-\frac{s \Lambda}{v}} \end{pmatrix}. \tag{33}$$

The vehicle system  $H(s)$  can be sampled as described in section 2.2 to find a digital *vehicle filter*. Alternatively, this filter can be found by calibrating the vehicle and analyzing its response (Zhu et. al., 2009). A bank of such digital vehicle filters can be used to represent the relevant traffic. The road height signals are determined by the road height profile and the speed of the vehicle. These signals are then filtered with vehicle filters to find the response of various vehicles, and with the lumbar spine filter in section 4.1.1 to find the human response. In this way, the health risk of road humps can be evaluated with digital filtering.

### 4.2 Road surface texture

The texture of roads is a critical feature. It affects the friction between the road surface and the tire. Slippery roads in rain are often a consequence of lack of texture of the road and/or the tire. If a road has been found to have insufficient texture, it must be modified to avoid accidents. Since it is very costly to rebuild roads, the pass and fail criteria are crucial. The surface texture is determined in two steps. The road surface is first measured and densely sampled, often with a *profilograph*. It is a vehicle equipped with a height measuring system. The vehicle motion is determined with inertial navigation and the distance between its height and the road is measured with a laser. The difference signal describes the road surface. The surface height map is then condensed into a feature called mean profile depth (MPD), according to an international standard (ISO 13473-1, 1997). Unfortunately, the evaluation lacks robustness. Independent evaluations may result in different values of the MPD. Hence, the method needs to be improved. The current evaluation is first described and commented in section 4.2.1. An improved method based on digital filtering will then be proposed in section 4.2.2. Digital filters are robust as they specify the calculation completely. Fixing the sampling rate, the proposed filter coefficients can be directly stated in a revised standard, similarly to the specification of the lumbar spine filter (ISO 2631-5, 2004).

#### 4.2.1 Mean profile depth (MPD)

The standard for characterization of road/pavement texture (ISO 13473-1, 1997) follows the steps in Fig. 12 to evaluate road height variations with wavelengths in the range of 5–50 mm, corresponding to a frequency band 20–200 m<sup>-1</sup>. Inverse distance is a frequency equivalent to inverse time.

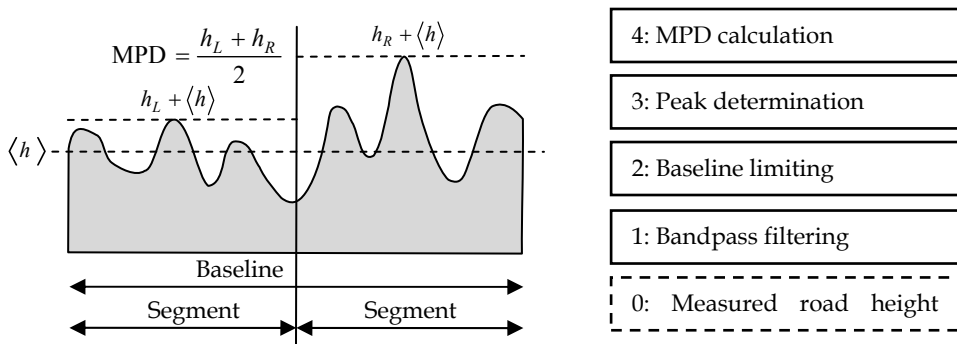


Fig. 12. The mean profile depth (MPD) (left) is according to the standard (ISO 13473-1, 1997) determined in four steps (right), using a measured map of heights  $h$  (Step 0).

The road height profile (step 0) must be sampled with a horizontal resolution of at least 1 mm. That is plausible considering the shortest wavelength of interest (5 mm). The bandpass-filtering (step 1) is not further specified than the -3 dB cross-over frequencies [10, 400]m<sup>-1</sup> and minimal slopes [6, 12]dB/octave. The upper cross-over frequency is on the borderline of being consistent with the sampling rate – the utilization is as high as 400/500 = 80%. The specification of *minimal slope* may be understood from the widespread

concept of ideal 'square' filter response in the frequency domain. It cannot be understood from considerations in the space domain: A too abrupt cut-off in the frequency domain must result in oscillations in the space domain. Further, in the space domain the phase distortion is important. No requirement on the phase response of the band-pass filter is however made. Baseline limiting (step 2) consists of dividing the measured surface profile into consecutive baseline intervals of  $100 \pm 10$  mm length. The peaks in the two adjacent segments of equal length (50 mm) are then detected (step 3). The MPD is finally determined as the average of these peaks, measured relative to the mean height (step 4).

Dividing the profile into baselines and detecting isolated peaks in this way may be common but is definitely not robust. The result is sensitive to translations of the dividing points of adjacent baselines, as well as changes in the position of the peaks. Any peak occurring only once in each segment will be counted in full but together with a larger peak, it will be completely neglected. These deficiencies will result in noisy MPD-signals.

#### 4.2.2 Modified MPD (MMPD)

Many aspects of the current standard can be improved without major deviations from the intentions of the standard. The degree of agreement between the modified mpd (MMPD) to be proposed and the current MPD will *not* be a measure of quality. Rather, the quality is to be found in fulfillment of the intentions of the current standard (ISO 13473-1, 1997) and desired properties such as low sensitivity to irrelevant disturbances, repeatability in independent evaluations and simplicity of implementation.

The band-pass filtering in step 1 (Fig. 12) describes the selection of relevant information. The filter needs to be specified in more detail to improve the repeatability as well as reducing the distortion. A simple method to eliminate phase distortion is to use symmetric forward and reversed digital filtering (section 2.1). The fall-off rate can be chosen as low as possible by using a first-order filter. The suggestion is to use a standard digital Butterworth filter of first order with cross-over frequencies  $[6.5, 434] \text{m}^{-1}$ , and apply it in both directions of space. A sampling rate  $f_s = 1000 \text{m}^{-1}$  complies with the required resolution and gives a numerically acceptable utilization. That will result in a fall-off rate of  $[12, 12] \text{dB/octave}$  and zero phase response. This filter fulfills all requirements of the current standard.

The MPD calculation requires major adjustments to become robust. The division into disjoint baselines (step 2, Fig. 12) is preferably substituted with overlapping baselines. Calculating the average height  $\langle h \rangle$  will then directly correspond to digital filtering of the road profile with an averaging FIR-filter with equal coefficients  $b_k = 1/100, k = 1, 2, \dots, 100$ . Averaging filters belong to the class of smoothing filters and are well-known to be anything but perfect (Hamming, 1998). They have an oscillating frequency response, an undesirable finite amplification at the Nyquist frequency  $f_N$ , as well as an unwanted finite slope at zero frequency. Applying an averaging filter is equivalent of piecewise linear regression with a constant. A better alternative is to use a polynomial. Such *polynomial smoothing FIR-filters* (includes the averaging filter) have linear phase (symmetric coefficients). Polynomial filters have the same deficiency of finite amplification at  $f_N$ . This undesired response may be removed by adjusting the identical first and last coefficients. Treating them as a free parameter they may be adjusted for zero gain of the filter at  $f_N$ . That will improve the high

frequency attenuation considerably, see Fig. 13 (right). The unavoidable change in bandwidth may be compensated by adjusting the length of the filter. These filters will be called *modified polynomial filters*. The regularity or differentiability at zero frequency increases with the order of the polynomial: An  $n$ -th order polynomial filter has  $n-1$  vanishing derivatives at zero frequency. Thus, they resemble the Butterworth 'max-flat' design (Hamming, 1998). The modified polynomial FIR filter is thus comparable to the IIR Butterworth filter, see Fig. 13 (left). Avoiding recursion requires many more coefficients – filters like the polynomial filters could be obtained by truncated sampling of the infinite impulse response of Butterworth filters. This truncation introduces oscillations as shown in Fig. 13 (right).

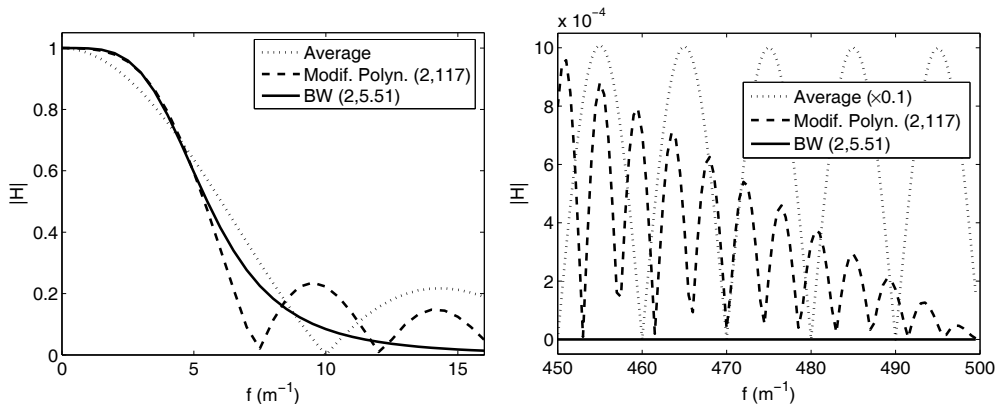


Fig. 13. Magnitude of frequency response of smoothing filters, in the low (left) and high (right) frequency range: the averaging filter (right:  $\times 0.1$ ), the modified square polynomial 117-tap FIR filter, and the proposed second order Butterworth filter (BW) with cross-over frequency  $5.5 \text{ m}^{-1}$ .

The smoother roll-off of the recursive Butterworth filter results in a more robust analysis of noisy measurements. Its low number of filter coefficients is also preferable in a standard document. The complexity of implementation is low as well as the risk of making errors. The order of filtering is not critical for the remaining steps of the analysis and can be increased. The phase distortion may once again be eliminated with symmetric forward and reverse filtering (section 2.1). The effective order will then double to four.

The peaks detected in step 3 (Fig. 12) are closely related to percentiles determined from cumulative probability distributions. Percentiles are for instance used in calibrations (ISO GUM, 1993). The  $n$ -th percentile  $P_n(\{x\})$  is the value exceeding precisely  $n$  per cent of all samples  $\{x\}$ . Statistical moments (section 3.3.2) are superior to high percentiles in robustness as they utilize weighing over *all* samples. The ratios of percentiles and the standard deviation are called coverage factors (section 3.3). A robust measure of peaks is found by combining a short-range standard deviation and a long-range percentile. The number of samples in every baseline is far too low for evaluation of percentiles. Each set of 100 consecutive recordings of the road depth in each baseline may be considered as samples drawn from a unique pdf. The widths of different pdfs belonging to different baselines are

likely different. The coverage factors or the types of these pdfs are likely much less different. A plausible assumption is that the coverage factors for different baselines are nearly equal and can be estimated using *all* samples. This global coverage factor is as robust as possible. The mean of the two peaks in Fig. 12 are rather well described by the 99–th percentile. The calculation of the standard deviation is robust enough to be calculated for each baseline. The smoothing filter used to calculate the mean baseline depth  $\langle h \rangle$  can also be used to evaluate the mean baseline square deviation  $\langle (h - \langle h \rangle)^2 \rangle = \langle h^2 \rangle - \langle h \rangle^2$ , or squared standard deviation. The smoothing filter is effectively a rather sharp anti-alias filter. The MPD signal may therefore be directly down-sampled to be consistent with the baseline resolution. This concludes the derivation of the method for determining the *modified MPD* (MMPD):

1. The measured road profile is sampled with  $f_s = 1000 \text{ m}^{-1}$ . Otherwise, linear down-sampling is applied.
2. The road profile is filtered in both directions of time with a digital band-pass Butterworth filter of order one with cross-over frequencies  $f_c = [6.5, 434] \text{ m}^{-1}$ . Filter coefficients<sup>2</sup>:  $b = [0.8119 \ 0 \ -0.8119]$ ,  $a = [1.000 \ -0.3099 \ -0.6237]$ .
3. The running mean and variance of the depth are evaluated with the same smoothing filter. The digital Butterworth filter is of order two, has a cross-over frequency  $f_c = 5.5 \text{ m}^{-1}$ , and is applied in both directions of time. The band-pass filtered road profile  $h$  and its square  $h^2$  are filtered to give  $\langle h \rangle_s$  and  $\langle h^2 \rangle_s$ , respectively. Filter coefficients:  $b = 10^{-3} \times [0.2921 \ 0.5842 \ 0.2921]$ ,  $a = [1.000 \ -1.9511 \ 0.9522]$ .
4. The 99–th percentile of the road depth,  $P_{99}(h - \langle h \rangle_A)$ , where  $\langle \cdot \rangle_A$  denotes *average over all samples*, will be called *GPD – Global Profile Depth*. It is a measure of the mean MMPD. The global coverage factor is given by,  $k_p = \text{GPD} / \sqrt{\langle h^2 \rangle_A - \langle h \rangle_A^2}$ .
5. The mean profile depth is given by,  $\text{MMPD} = \text{GPD} \times \sqrt{\langle h^2 \rangle_s - \langle h \rangle_s^2} / \sqrt{\langle h^2 \rangle_A - \langle h \rangle_A^2}$ .
6. Finally, the MMPD is down-sampled to  $f_s = 20 \text{ m}^{-1}$ .

An example of calculated MMPD is shown in Fig. 14. The generated road profile was an uncorrelated normally distributed variation of depth with standard deviation equal to one. The smoothing filter of the MMPD is compared to the average filter suggested by the current standard. Clearly, the robustness improved considerably – the noise of the calculated mean profile depth disappeared.

---

<sup>2</sup> Defined according to a common convention (Matlab): Numerator  $b = [b_0 \ b_1 \ \dots]$  and denominator  $a = [a_0 \ a_1 \ \dots]$ , where the indices denote the lag in samples.

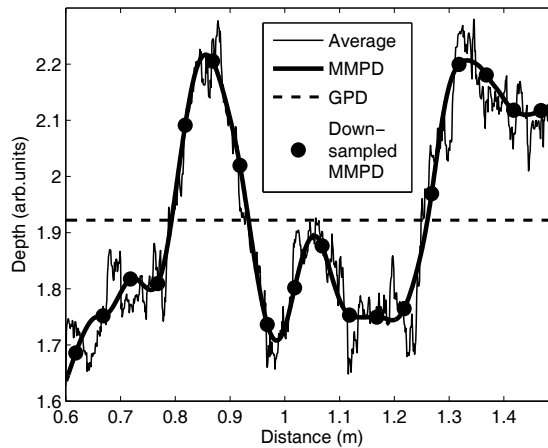


Fig. 14. The proposed smoothing of the MMPD compared to the average smoothing of the present MPD, for an uncorrelated normally distributed road profile.

## 5. Conclusions

A multitude of different digital filters for exploring and refining measurements have been discussed: single correction filters or ensembles of correction filters, sensitivity filters, lumbar spine filter, banks of vehicle filters, and road texture filters. The analyses they realize differ substantially. All digital filters were designed or synthesized in three steps: dynamic model – prototype – digital filter. The identification of models was not considered as a part of the synthesis of digital filters and was omitted. The model describes the physical system and the prototype what we are interested in. The major part of the chapter focused on the construction of prototypes from models. The prototypes were sampled into digital filters. A brief survey of some well established sampling techniques was given. In the examples, prototypes were sampled with the exponential pole-zero mapping.

The discussed filters fell into one of two categories: 1. Analysis of measured signals utilizing calibration information of the measurement system. 2. Extraction of any feature of interest that is related to a measured signal. Digital filters devised to correct and analyze measured signals are preferably considered as a part of an improved measurement system. The extracted feature could be a constant like an accumulated dose describing the risk of injury, or a spatially varying measure of road texture. A feature is justified by its broad acceptance and they are therefore often defined in standard documents. A feature which is not robust is questionable and may lose its importance. Low robustness originates from the definition of the feature and/or its incomplete specification. In this context digital filters are ideal, as they completely describe how the extraction is made with a finite set of numerical numbers. Many operations are difficult to realize in real time, like zero-phase filtering and stabilization. These become trivial with reversed filtering, as was illustrated repeatedly. The only example of non-linear digital filtering, the human lumbar spine filter, was analyzed but not synthesized. It is strongly desired that measurement systems are as linear-in-response as possible. Correction of the non-linear response of measurement systems with

non-linear digital filters is virgin territory. It requires non-linear model identification, which needs to be further developed to reach the 'off-the-shelf' status of linear identification methods. The sampling techniques for linear systems can to some extent probably be inherited to sampling of non-linear prototypes.

A challenge for the future is to find novel and unique applications where digital filters really make a difference to how measurements are processed into valuable results. Digital filters are dynamic time-invariant systems with feedback. That sets their potential but also their limitations. Sampling is separate from construction of prototypes. Even though sampling of systems always introduces errors, it seldom limits the performance of digital filters. Normally, it is the quality of the underlying model that is crucial. A digital filter can never perform better than the model from which its prototype is constructed.

Differential equations in time are ubiquitous and are used in perhaps the majority of all physical and technological models, but rarely for calibrating measurement systems. For all such models, digital filters are potential candidates for modeling, refining results and extracting information. Digital filters supporting measurements and synthesized by a third-party (neither manufacturers, nor users) are still in their infancy. It is truly amazing how useful such digital filters often turn out to be in various applications.

## 6. References

- Björk, A. (1996). *Numerical methods for least squares problems*, Siam, ISBN-13: 978-0-898713-60-2 / ISBN-10: 0-89871-360-9, Philadelphia
- Bruel&Kjaer (2006). Magazine No. 2 / 2006, pp. 4-5;  
<http://www.bksv.com/products/pulseanalyzerplatform/pulsehardware/rexresponseequalisation.aspx>
- Chen, C. (2001). *Digital Signal Processing*, Oxford University Press, ISBN 0-19-513638-1, New York
- Crossway, F.L. & Kalb, H.T. (1970). Dynamic Force Measurement Techniques, *Instruments and Control Systems*, Febr. 1970, pp. 81-83
- Ekstrom, M.P. (1972). Baseband distortion equalization in the transmission of pulse information, *IEEE Trans. Instrum. Meas.* Vol. 21, No. 4, pp. 510-5
- Elster, C.; Link, A. & Bruns, T. (2007). Analysis of dynamic measurements and determination of time-dependent measurement uncertainty using a second-order model, *Meas. Sci. Technol.* Vol. 18, pp. 3682-3687
- Engwall, B. (1979). Device to prevent vehicles from passing a temporarily speed-reduced part of a road with high speed, United States Patent 4135839
- Gustafsson, F. (1996). Determining the initial states in forward-backward filtering, *IEEE Trans. Sign. Proc.*, Vol. 44, No. 4, pp. 988-992
- Hale, P.D. & Dienstfrey, A. (2010). Waveform metrology and a quantitative study of regularized deconvolution, *Instrum. Meas. Technol. Conf. Proc. 2010, I2MTC '10, IEEE*, Austin, Texas
- Hamming, R.W. (1998). *Digital filters*, Dover/Lucent Technologies, ISBN 0-486-65088-X, New York
- Hessling, J.P. (2006). A novel method of estimating dynamic measurement errors, *Meas. Sci. Technol.* Vol. 17, pp. 2740-2750
- Hessling, J.P. (2008a). A novel method of dynamic correction in the time domain, *Meas. Sci. Technol.* Vol. 19, pp. 075101 (10p)

- Hessling, J.P. (2008b). Dynamic calibration of uni-axial material testing machines, *Mech. Sys. Sign. Proc.*, Vol. 22, 451-66
- Hessling, J.P. & Zhu, P.Y. (2008c). Analysis of Vehicle Rotation during Passage over Speed Control Road Humps, *ICICTA 2008, International Conference on Intelligent Computation Technology and Automation*, Changsha, China, Oct. 20-22, 2008.
- Hessling, J.P. (2009). A novel method of evaluating dynamic measurement uncertainty utilizing digital filters, *Meas. Sci. Technol.* Vol. 20, pp. 055106 (11p)
- Hessling, J.P. (2010a). *Metrology for non-stationary dynamic measurements, Advances in Measurement Systems*, Milind Kr Sharma (Ed.), ISBN: 978-953-307-061-2, INTECH, Available from: <http://sciendo.com/articles/show/title/metrology-for-non-stationary-dynamic-measurements>
- Hessling, J.P.; Svensson, T. & Stenarsson, J. (2010b). Non-degenerate unscented propagation of measurement uncertainty, submitted for publication
- Hessling, J.P. (2010c). Unscented binary propagation of uncertainty, in preparation
- ISO 2631-5 (2004). *Evaluation of the Human Exposure to Whole-Body Vibration*, The International Organization for Standardization, Geneva
- ISO 13473-1 (1997). *Characterization of pavement texture by use of surface profiles – Part 1: Determination of Mean Profile Depth*, The International Organization for Standardization, Geneva
- ISO GUM (1993). *Guide to the Expression of Uncertainty in Measurement*, 1<sup>st</sup> edition, International Standard Organization, ISBN 92-67-10188-9, Geneva
- Julier, S.; Uhlmann, J. & Durrant-Whyte, H. (1995). A new approach for filtering non-linear systems, *American Control Conference*, pp. 1628-1632
- Julier, S. & Uhlmann, J.K. (2004). Unscented Filtering and Nonlinear Estimation, *Proc. IEEE*, Vol. 92, No. 3, (March 2004) pp. 401-422
- Ljung, L. (1999). *System Identification: Theory for the User*, 2<sup>nd</sup> Ed, Prentice Hall, ISBN 0-13-656695-2, Upper Saddle River, New Jersey
- Matlab with System Identification, Signal Processing Toolbox and Simulink, The Mathworks, Inc.
- Metropolis, N. & Ulam, S. (1949). The Monte Carlo Method, *Journal of the American Statistical Association*, Vol. 44, No. 247, pp 335-341
- Moghisi, M. & Squire, P.T. (1980). An absolute impulsive method for the calibration of force transducers, *J. Phys. E.: Sci. Instrum.* Vol. 13, pp. 1090-2
- Pintelon, R. & Schoukens, J. (2001). *System Identification: A Frequency Domain Approach*, IEEE Press, ISBN 0-7803-6000-1, Piscataway, New Jersey
- Pintelon, R.; Rolain, Y.; Vandeen Bossche, M. & Schoukens, J. (1990). Toward an Ideal Data Acquisition Channel, *IEEE Trans. Instrum. Meas.* Vol. 39, pp. 116-120
- Rubenstein, R.Y. & Kroese, D.P. (2007). *Simulation and the Monte Carlo Method* (2<sup>nd</sup> Ed.) John Wiley & Sons ISBN 9780470177938
- Simon, D. (2006). *Optimal State Estimation: Kalman,  $H_\infty$  and non-linear approaches*, Wiley, ISBN-13 978-0-471-70858-2, New Jersey
- Wiener, N. (1949). *Extrapolation, Interpolation, and Smoothing of Stationary Time Series*, Wiley, ISBN 0-262-73005-7, New York;  
[http://en.wikipedia.org/wiki/Wiener\\_deconvolution](http://en.wikipedia.org/wiki/Wiener_deconvolution)
- Zhu, P.Y.; Hessling, J.P. & Wan, R. (2009). Dynamic Calibration of a bus, *Proceedings of XIX IMEKO World Congress*, Lisbon, Portugal Sept., 2009



## **Digital Filters**

Edited by Prof. Fausto Pedro García Márquez

ISBN 978-953-307-190-9

Hard cover, 290 pages

**Publisher** InTech

**Published online** 11, April, 2011

**Published in print edition** April, 2011

The new technology advances provide that a great number of system signals can be easily measured with a low cost. The main problem is that usually only a fraction of the signal is useful for different purposes, for example maintenance, DVD-recorders, computers, electric/electronic circuits, econometric, optimization, etc. Digital filters are the most versatile, practical and effective methods for extracting the information necessary from the signal. They can be dynamic, so they can be automatically or manually adjusted to the external and internal conditions. Presented in this book are the most advanced digital filters including different case studies and the most relevant literature.

### **How to reference**

In order to correctly reference this scholarly work, feel free to copy and paste the following:

Jan Peter Hessling (2011). Integration of Digital Filters and Measurements, Digital Filters, Prof. Fausto Pedro García Márquez (Ed.), ISBN: 978-953-307-190-9, InTech, Available from:

<http://www.intechopen.com/books/digital-filters/integration-of-digital-filters-and-measurements>

# **INTECH**

open science | open minds

### **InTech Europe**

University Campus STeP Ri  
Slavka Krautzeka 83/A  
51000 Rijeka, Croatia  
Phone: +385 (51) 770 447  
Fax: +385 (51) 686 166  
[www.intechopen.com](http://www.intechopen.com)

### **InTech China**

Unit 405, Office Block, Hotel Equatorial Shanghai  
No.65, Yan An Road (West), Shanghai, 200040, China  
中国上海市延安西路65号上海国际贵都大饭店办公楼405单元  
Phone: +86-21-62489820  
Fax: +86-21-62489821

© 2011 The Author(s). Licensee IntechOpen. This chapter is distributed under the terms of the [Creative Commons Attribution-NonCommercial-ShareAlike-3.0 License](#), which permits use, distribution and reproduction for non-commercial purposes, provided the original is properly cited and derivative works building on this content are distributed under the same license.